AD-A061 910 NAVAL RESEARCH LAB WASHINGTON D C F/G 4/1
ESTIMATING THE SPECTRUM OF ELECTRON DENSITY FLUCTUATIONS FROM S--ETC(U)
JUL 78 N J ZABUSKY, J BLOCK
UNCLASSIFIED NRL-MR-3586 NL

1 OF 1
AD
A061910

END
DATE
FILMED
2 79
DDC

NRL Memorandum Report 3586

Estimating the Spectrum of Electron Density Fluctuations from Simulations of Ionospheric Plasma Clouds

NORMAN J. ZABUSKY AND JOSEPH BLOCK

Geophysical and Plasma Dynamics Branch
Plasma Physics Division

July 1978

This research was sponsored by the Defense Nuclear Agency under *DNA Subtask* S99QAXHCO41;
Work Unit Code 12, Title "Ionization Structured Research."

NAVAL RESEARCH LABORATORY
Washington, D.C.

Approved for public release; distribution unlimited.

SECURITY CLASSIFICATION OF THIS PAGE (When Data Entered)

REPORT DOCUMENTATION PAGE		READ INSTRUCTIONS BEFORE COMPLETING FORM
1. REPORT NUMBER (14) NRL-MR- NRL Memorandum Report 3586	2. GOVT ACCESSION NO.	3. RECIPIENT'S CATALOG NUMBER (9)
4. TITLE (and Subtitle) (6) ESTIMATING THE SPECTRUM OF ELECTRON DENSITY FLUCTUATIONS FROM SIMULATIONS OF IONOSPHERIC PLASMA CLOUDS *		5. TYPE OF REPORT & PERIOD COVERED Interim report, ~~on a continuing~~ NRL problem
		6. PERFORMING ORG. REPORT NUMBER
7. AUTHOR(s) (10) Norman J. Zabusky* Joseph Block†		8. CONTRACT OR GRANT NUMBER(s) NRL Problem No. H02-27B DNA Subtask S99QAXHCO41 (16)
9. PERFORMING ORGANIZATION NAME AND ADDRESS Naval Research Laboratory Washington, DC 20375		10. PROGRAM ELEMENT, PROJECT, TASK AREA & WORK UNIT NUMBERS NRL Problem No. H02-27B Project DNA S99QAXHCO41
11. CONTROLLING OFFICE NAME AND ADDRESS Defense Nuclear Agency Washington, DC 20305		12. REPORT DATE (11) July 1978 (17) C041
		13. NUMBER OF PAGES 68
14. MONITORING AGENCY NAME & ADDRESS(if different from Controlling Office) (12) 69p.		15. SECURITY CLASS. (of this report) UNCLASSIFIED
		15a. DECLASSIFICATION/DOWNGRADING SCHEDULE

16. DISTRIBUTION STATEMENT (of this Report)

Approved for public release; distribution unlimited.

17. DISTRIBUTION STATEMENT (of the abstract entered in Block 20, if different from Report)

18. SUPPLEMENTARY NOTES

This research was sponsored by the Defense Nuclear Agency under DNA Subtask S99QAXHCO41; Work Unit Code 12, Title "Ionization Structured Research." *Permanent Address: Depts. of Mathematics & Electrical Engineering, Univ. of Pittsburgh, Pittsburgh, Pa. 15260. †Naval Research Laboratory, Space Systems Division, Advance Planning Group, Washington, DC 20375.

19. KEY WORDS (Continue on reverse side if necessary and identify by block number)

Ionospheric plasma clouds
Electron density fluctuations
Power spectrum
Simple striation shapes
Numerical simulation

20. ABSTRACT (Continue on reverse side if necessary and identify by block number)

For electron density fluctuations of area $\mathcal{A}$ that are nearly piecewise constant and have well-separated scales, the amplitude of the spectrum $\hat{f}(\underline{k})$ at large wave numbers ($k\mathcal{A}^{1/2} >> 1$) is proportional to the $P/\mathcal{A}$. The perimeter P is associated with the length of the boundary of the steep "sides" of the cloud and its cleavages. Thus,

$$\hat{n} \propto (P/\mathcal{A})k^{-1},\ k\,\mathcal{A}^{1/2} >> 1.$$

(Continued)

DD FORM 1 JAN 73 1473 EDITION OF 1 NOV 65 IS OBSOLETE
S/N 0102-014-6601

SECURITY CLASSIFICATION OF THIS PAGE (When Data Entered)

251 950

78 12 06 014

20. ABSTRACT: (Continued)

This important fact is deduced from analytical considerations of model figures with well-separated scales.

Using a combination of analytic concepts and sample numerical calculations, we also deduce that only 40% of the modes are useful for estimating the exponent *p* in a power-law fit to the one-dimensional spectrum of electron density fluctuations (EDF's) obtained in numerical simulations. The remaining 60% of the modes provide support for the numerical simulations and are subject to various errors.

CONTENTS

ESTIMATING THE SPECTRUM OF ELECTRON DENSITY FLUCTUATIONS FROM SIMULATIONS OF IONOSPHERIC PLASMA CLOUD

I. INTRODUCTION

Numerical simulations of ionospheric plasma clouds yield information for four related purposes:

(1) To interpret past barium cloud experiments;

(2) To predict phenomena in new experiments;

(3) To validate algorithms used in system codes which determine the life-time of sky regions occluded by striations following a nuclear explosion; and

(4) To predict the temporal evolution of the spectrum of electron-density fluctuations (EDF's) for use in propagation studies.

In this memorandum we study the spectrum of simple geometric figures that have shapes similar to those that arise in the evolution of ionospheric plasma clouds.

The evolution of large plasma clouds is at least a two-dimensional intrinsically nonlinear process. Essentially, we are studying the evolution of a deformable dielectric where each element of the dielectric is convected by a velocity proportional to the local electric field. The process is more complex if the ionosphere is compressible, if recombination chemistry processes are important and if the neutral wind varies with altitude. At present, even in the simplest cases, we must resort to computer simulations to obtain answers to the questions posed above. With our present understanding we may divide a cloud's evolutionary history into several overlapping time phases:

(1) Steepening of an initially smooth cloud;

(2) Distortion at an angle to the **E** × **B** drift velocity;

(3) Cleavage into strips or "fingers" of ionization[1,2,3];

(4) Bifurcation-and-pinching of strips;

Manuscript submitted June 26, 1978.

(5) Decay of small field-aligned "rods" of ionization.

Thus, the "cascade" to smaller scale lengths is due essentially to cleavage, bifurcation and pinching.

In numerical simulations, it has been observed that the "sides" of the cleavage-produced indentations and protuberances can be very steep[1,2,3] Thus, almost from the beginning, there will be electron density fluctuations that affect propagation. With increasing elapsed time, more of the cloud will be affected and the amplitude of these high wave-number components will increase until some near-steady state is achieved.

In the next section we examine the spectrum of a variety of simple and composite geometric figures and conclude that the *amplitude* of the spectrum at large wavenumber is proportional to the *perimeter* of these figures. Thus, the more tortuous is the backside boundary, the larger is the amplitude.

In the final section, we examine one-dimensional discrete spectra and conclude that only an intermediate 40% of the modes can be trusted to deduce a power spectrum from a particular numerical simulation with periodic boundary conditions. The remainder of the modes are needed for the support of the computation. The lowest (long-wavelength) modes are slightly distorted because of artificially imposed boundary conditions (in our case periodic boundary conditions). The highest 40-50% of the modes are in error for several reasons. First, the spatial and temporal discretization methods for solving the nonlinear partial differential equations are usually second-order; second, artificial nonlinear damping is usually inserted if the true evolutionary processes give rise to steep structures; and finally, for a fixed-interval mesh with periodic boundary conditions, we in effect are sampling a periodic function and introducing aliasing errors that result from "folding back" modes.[4]

II. POWER SPECTRUM OF ELECTRON DENSITY FLUCTUATIONS: ANALYTICAL CONSIDERATIONS

On the basis of the continuous and discrete one-and two-dimensional Fourier transforms

of simple geometric figures, we present insights into the parameters that control the amplitude and power-law dependence of EDF's. In particular, we show that at long wavelengths the *area* of EDF's controls the amplitude while at short wavelengths it is the *perimeter* of steep regions that controls the amplitude. The existence of a "power law" spectrum of EDF's depends upon the separation of space scales.

A. One-Dimensional Continuous Transforms

We first examine the energy spectrum of two one-dimensional rectangular functions as shown in Fig. 1. This will serve to illustrate the idea that at small k the "area" determines the amplitude of the spectrum whereas at large k the perimeter controls the amplitude.

In one-dimension the direct and inverse Fourier transform are

$$\hat{f}(k) = \int_{-\infty}^{+\infty} f(x)\, e^{-ikx}\, dx, \tag{1}$$

and

$$f(x) = \left(\frac{1}{2\pi}\right) \int_{-\infty}^{+\infty} \hat{f}(k)\, e^{+ikx}\, dk, \tag{2}$$

and Parseval's theorem gives[5]

$$\int_{-\infty}^{+\infty} |\hat{f}|^2\, dk = 2\pi \int_{-\infty}^{+\infty} f^2(x)\, dx. \tag{3}$$

For the function given in Fig. 1,

$$\hat{f} = 4LA \left(\frac{\sin z}{z}\right) \cos mz\, e^{-imz}, \tag{4}$$

where $z = kL$.

Thus, the integrated energy spectrum in the region from k_o to ∞ is

$$\begin{aligned} IES(k_o) &= \int_{k_o}^{\infty} \hat{f}\hat{f}^*\, dk = 16LA^2 \int_{z_o}^{\infty} \frac{(\sin \xi \cos m\xi)^2}{\xi^2}\, d\xi \\ &= 16\, LA^2 \left\{ \frac{1}{4}\pi + \frac{1}{z} (\sin z \cos mz)^2 \right. \\ &\quad - \frac{1}{4} \Big[m_+ Si(2m_+ z) + m_- Si(2m_- z) \\ &\quad \left. + 2\, Si(2z) - 2m\, Si(2mz) \Big] \right\}, \end{aligned} \tag{5}$$

where

$$m_{\pm} = m \pm 1 \quad \text{and} \quad Si(z) = \int_0^z \frac{\sin x}{x}\, dx. \tag{6}$$

At $k = 0$

$$IES(0) = 4\pi LA^2, \tag{7}$$

a result obtained from Parseval's theorem. Now if we take $z = n\pi > 1$ then

$$IES(n\pi) = \frac{2LA^2}{n\pi} + O(n\pi)^{-3}, \qquad (m = 1),$$

$$IES(n\pi) = \frac{4LA^2}{n\pi} + O(n\pi)^{-3}, \qquad (m > 1). \tag{8}$$

That is, the coefficient of $(LA^2/n\pi)$ is a number indicating the total number of discontinuities of the well-separated rectangular functions. This implies that there is a redistribution of energy in k space, while the total energy $=$ IES$(0)/\pi$, is constant. In two dimensions, we will see that the perimeter of the figures corresponds to the total number of discontinuities in one dimension.

B. Two-Dimensional Continuous Transforms

Fig. 2 shows the pill-box $f_P(x)$ and the frustum of a cone $f_F(x)$ that we consider as basic figures to represent two dimensional clouds. These figures have enough parameters to provide realistic models of EDF's and their symmetry allows an easy interpretation of formulas in asymptotic limits.

If we define the Fourier transform $\hat{f}(\mathbf{k})$ as

$$\hat{f}(\mathbf{k}) = \int_{-\infty}^{+\infty} \int_{-\infty}^{+\infty} dx\, dy\, f(x)\, e^{-i\mathbf{k}\cdot\mathbf{x}}, \tag{9}$$

$$= \int_0^{2\pi} d\phi \int_0^{\infty} r f(r) e^{ikr\cos(\theta-\phi)}\, dr, \tag{10}$$

where

$$\mathbf{k}\cdot\mathbf{x} = kr\cos(\theta - \phi),$$

since $k_1 = k\cos\theta$, $k_2 = k\sin\theta, x = r\cos\phi$ and $y = r\sin\phi$. For figures with azimuthal symmetry we may write

$$\hat{f}(k) = 2\pi \int_0^{\infty} r f(r)\, J_0(kr)\, dr. \tag{11}$$

For the pill box and the frustum of a cone we obtain, respectively

$$\hat{f}_P = A(2\pi R^2)\, J_1(z)/z, \tag{12}$$

$$\hat{f}_F = A 2\pi R^2 [z^{-2} (z_o - z)^{-1}] \left[zJ_o(z) - z_o J_o(z_o) + \int_z^{z_o} J_o(z')\, dz' \right], \tag{13}$$

where $z = kR$, $z_o = kR_o$. Note, that the Fourier transform of these isolated figures with azimuthal symmetry are real.

We define the one-dimensional energy spectrum $E(k)$ as

$$E(k) = k \int_0^{2\pi} \hat{f}(\mathbf{k}) \hat{f}(\mathbf{k})^* \, d\theta \tag{14}$$

and we obtain the asymptotic limits:

small kR

$$E_P = A^2 2\pi k [\pi R^2]^2, \tag{15a}$$

$$E_F = A^2 2\pi k \left[\frac{1}{3} \pi (R^2 + RR_o + R_o^2) \right]^2; \tag{15b}$$

large kR

$$E_P = A^2 16\pi^2 R \; (k^{-2}) \; [\cos(kR - 3\pi/4)]^2 + O(kR)^{-3}, \tag{16a}$$

large kR and kR_o

$$E_F = A^2 16\pi^2 \; (R_o/\delta^2) \; (k^{-4}) \left[\cos\left[kR_o - \frac{1}{4}\pi \right] - \left[\frac{R}{R_o} \right]^{1/2} \cos \left[kR - \frac{1}{4}\pi \right] \right]^2$$
$$+ \; O \left[(kR)^{-5}, \; (kR_o)^{-5} \right], \tag{16b}$$

where $\delta = R_o - R$. If $\delta << R_o$, Eq. (16b) can be written as

$$E_F = A^2 16\pi^2 (R_o/\delta^2) \; (k^{-4}) \left\{ (2 \sin \frac{1}{2} k\delta) \cos \left[kR_o - \frac{1}{2} k\delta - \frac{3\pi}{4} \right] \right.$$
$$\left. - \frac{1}{2} (\delta/R) \cos (kR - \pi/4) + O(\delta^2/R^2) \right\}^2 + O(kR)^{-5}. \tag{17}$$

Several features of $E(k)$ deserve comment. At small kR, the "volume" (($A^2 \times$ effective area) of the elementary figures, Eqs (15a) and (15b), is recovered as we expect from Parseval's theorem. At $(kR) >> 1$, the pill-box function has a *modulated* power-law dependence k^{-p} with $p = 2$ and k-period $2\pi/R$. At $(kR, kR_o) >> 1$ the function with the linear "skirts" and $\delta/R << 1$ has a *doubly* modulated power-law dependence with $p = 4$ and k-periods $4\pi/\delta$ and approximately $4\pi/(R_o + R)$.

If $(\delta/R) << k\delta << 1$ then the leading term of (17) is dominant, or

$$E_F = A^2 16\pi^2(R_o k^{-2}) \left\{\cos\left(kR_o - \frac{1}{2}k\delta - 3\pi/4\right) + O(k\delta)^2 + O(\delta/R)^2\right\}^2. \quad (18)$$

That is, if the space scales are well-separated, there is an intermediate region where E_F has a k^{-2} dependence. Now if one sets $R = R_o$ $(\delta = 0)$, we recover Eq. (16a). Note, if the linear skirts were replaced by a polynomial of degree "d", then the large-k power-law dependence would be $k^{-2(d+1)}$, that is $p = 2(d+1)$.

C. Energy Spectrum of M Pill-Boxes

If we have M azimuthally symmetric figures $f_m(\mathbf{x})$ whose centers of area are at $\mathbf{x}_m = \mathbf{e}_x x_m + \mathbf{e}_y y_m$, then the Fourier transform of the set is given by

$$f_M = \sum_{m=1}^{M} f_m(\mathbf{k})\, e^{-i\mathbf{k}\cdot\mathbf{x}_m},$$

and the one-dimensional energy spectrum, $E_M(k) = k\int_0^{2\pi}\left|\hat{f}_M\right|^2 d\theta$, is

$$E_M(k) = 2\pi\, k\sum_{m=1}^{M} |\hat{f}_m(k)|^2 + 4\pi k\sum_{m\neq n=1}^{M} |f_m f_n^*| J_o(kr_{mn}), \quad (19)$$

where $r_{mn} = \left[(x_m - x_n)^2 + (y_m - y_n)^2\right]^{1/2}$ and the Bessel function J_o arises by integrating over $\theta = \tan^{-1}(k_2/k_1)$, namely

$$\int_0^{2\pi} \exp\left[-\,ikr_{mn}(\cos\theta\cos\phi_{mn} + \sin\theta\sin\phi_{mn})\right] = 2\pi\, J_o(kr_{mn}),$$

where $\phi_{mn} = \tan^{-1}\left[(y_m - y_n)/(x_m - x_n)\right]$.

Now consider M *identical* pill-boxes of radius R_m. At *small-k* the self-interaction terms contribute $E_{M,\,\mathrm{self}} = MA_m^2\, 2\pi^3\, R_m^4\, k$ and the cross-interaction terms contribute $E_{M,\,\mathrm{cross}} = M(M-1)\, A_m^2\, 2\pi^3\, R_m^4\, k$ and thus the total is

$$E_M = A_m^2(2\pi^3)\,(M^{\frac{1}{2}}R_m)^4 k, \quad (\text{small } kR_m). \quad (20)$$

At *large-k* the self-interaction terms contribute $E_{M,\,\mathrm{self}} = A_m^2 16\pi^2(MR_m)k^{-2}\cos^2\left|kR_m - \frac{3\pi}{4}\right|$

and the cross-interaction terms contribute

$$E_{m,\,\mathrm{cross}} = A_m^2 16\pi^2\,(2/\pi)^{1/2}\,R_m^{1/2}k^{-(5/2)}\sum\sum_{m\neq n=1}^{M}\cos^2\left[kR - \frac{3\pi}{4}\right]\cos\left[kr_{mn} - \frac{\pi}{4}\right].$$

This term can be neglected because it falls-off more rapidly at large-k. Hence

$$E_M = A_m^2 16\pi^2 (MR_m) k^{-2} \cos^2(kR_m - 3\pi/4), \qquad \text{(large } kR_m\text{)}. \qquad (21)$$

Thus, if we take one pill-box of radius R and height $A=1$ and divide it into M pill boxes of radius $R_m = R/M^{1/2}$ (that is, preserving total area) then the 1-D energy spectrum is the same at small-k

$$E_M = (2\pi^3)\ R^4\ k, \qquad (kR << 1)$$

but at large-k the spectrum is

$$E_M = M^{1/2}\left\{16\pi^2\ Rk^{-2} \cos^2\left[kRM^{-1/2} - \frac{3\pi}{4}\right]\right\}, \qquad (kR >> M^{1/2})$$

namely $M^{1/2}$ times larger. From the above considerations, one may conjecture that at large-$k\bar{R}$ the *amplitude* of the one-dimensional energy spectrum is proportional to the *perimeter-to-area* ratio of a piecewise constant figure, where $\bar{R}\ \alpha\ (\mathcal{A})^{1/2}$ Thus, if we were to modulate the boundary of the pill-box function with $b_m \cos m\alpha$ ($b_m < \bar{R}$ and α is the polar angle) as depicted in Fig. 2c, we would expect to find a rise in $E(k)$ at $k \simeq m/\bar{R}$ with an amplitude proportional to the total perimeter $P = \int_o^{2\pi} ds$, as shown in Fig. 2f.

D. Computational Examples of One-Dimensional Energy Spectra

We illustrate the properties of some of the formulas of the preceding section in Figs. 3-6. Fig. 3 shows the spectrum of a single pill-box of radius π, Eq. (12). For $k < 0.1$ the spectrum grows linearly in k with a slope proportional to the area. At $k \simeq 0.4 (= 0.4\pi/R)$ the spectrum is a maximum and the modulated power-law spectrum begins. Several modulations are plotted and the k^{-2} power-law dependence is obtained by plotting Eq. (12) at k intervals $\Delta k = 2\pi/R = 2$. Fig. 4a shows $E(k)$ for two touching pill-boxes, namely $r_{12} = 2\pi$, and each of radius π. The asymptotic power-law dependencies are the same as previously, but the small-k region is shifted up by a factor of 4 while the large-k region is shifted up by a factor of 2, consistent with Eqs. (20) and (21), respectively. The maximum occurs at $k \simeq 0.25$ down from 0.4. The slanted arrow points to an indentation which is the first sign of interference effects. Fig. 4b, for $M = 2$, $r_{12} = 5\pi$ and $R = \pi$, shows the same asymptotic behavior as in Fig. 4a. However, the

maximum region is strongly modulated by interference effects. This is more pronounced in Fig. 4c for $M = 2$, $r_{12} = 10\pi$, and $R = \pi$ where the leading minimum at $k \simeq 0.1$ $[= (0.8\pi)/(r_{12} - 2R)]$ is decreased by a factor of ~ 2.0 from Fig. 4b. Note also, there are now three large maxima due to interference effects. Thus, the inclusion of many *identical* pill boxes does not change the asymptotic envelopes (k^{+1} or k^{-2}) including the maxima of the modulation. The region beginning at $k_{min} = \text{Max}\,(r_{12}-2R)^{-1}$ is modulated due to interference effects. If a large number of different radii were used to calculate the energy spectrum the modulation nulls would be "filled" and the asymptotic power-law dependencies would prevail.

Figs. 5a, 5b, and 5c show one-dimensional energy spectra for a frustum of a cone with inner radius $R = \pi$ and outer radii, $R_o = 1.1, 1.01\,\pi$ and $1.001\,\pi$, respectively The low-k regions are identical. The transition point, k_{tr}, from a k^{-2} spectrum to a k^{-4} spectrum is taken as the intersection of the two lines drawn tangent to the maxima (see the single vertical arrow). It moves to higher k with decreasing $\delta = R_o - R$, namely $k_{tr}\,\delta \simeq \frac{1}{2}\,\pi$. (Note, for $k > 8$ we have not plotted every point, but have sampled the function at equispaced intervals. In Fig. 5b, this accounts for the smooth behavior of the curve at $k \sim 50$ and the saw-tooth behavior for $k > 100$. For Fig. 5c, a similar comment applies for $k > 30$ and $k \sim 500$.) Figure 6 shows the one-dimensional energy-spectrum of two frustums $A = 1$, $R = \pi$, $R_o = 1.01\pi$ (like Fig. 5a) and $r_{12} = 10\pi$. The transition point $k_{tr} \simeq 60$ is increased slightly and except for the expected increase in amplitude, the large-k regions are identical. The low-k region shows a deep null and four maxima, similar to Fig. 4c.

III. DISCRETE FOURIER TRANSFORMS AND ENERGY SPECTRA OF FIGURES IN PERIODIC REGIONS

A. Analytical Results in One Dimension

Most numerical simulations of ionospheric plasma clouds are done with finite-difference methods on a periodic mesh. Thus, we now consider and compare the continuous and discrete periodic Fourier transforms of the trapezoidal figures shown in Fig. 7. The continuous

transform is

$$\hat{f}(k) = \int_{-L}^{L} f(x)e^{-ikx}\,dx = A\,(\beta+\alpha)\,L\left\{\frac{\sin z_+}{z_+}\;\frac{\sin z_-}{z_-}\right\}, \tag{22}$$

where $z_\pm = \frac{1}{2}\,kL(\beta \pm \alpha)$ and $k = \pi\nu/L,\ \nu = 1,2\ \cdots$. The first null is at $k_{n1} = 2\pi/(\beta+\alpha)L$ and at large k we have a function proportional to k^{-2} modulated at two frequencies, the slower associated with the width of the skirts, $(\beta-\alpha)L$. This is the one-dimensional version of the frustum of a cone treated earlier. The *discrete* Fourier transform $\hat{F}(k)$ on an interval $-N+1 \leqslant n \leqslant N$ is

$$\hat{F}(k) = \sum_{n=-N+1}^{n=N} f(nh)e^{-iknh},$$

$$= A(b+a)\left\{\frac{\sin\frac{1}{2}\,\theta(b-a)}{(b-a)\sin\frac{1}{2}\,\theta}\;\frac{\sin\frac{1}{2}\,\theta(b+a)}{(b+a)\sin\frac{1}{2}\theta}\right\}, \tag{23}$$

where $\theta = hk = (\pi\nu/N)$, and $\nu = (-N+1),\ \cdots\ -1,0,1,\ \cdots\ N.$

That is, the discrete system has $2N$ independent modes and Parseval's theorem has the form

$$\sum_{n=-N+1}^{N} f^2(nh) = 2N\sum_{\nu=-N+1}^{N}\hat{F}(k)\hat{F}^*(k). \tag{24}$$

Note, the highest mode available to the discrete system is $k = \pi/h$ and the lowest is $k = \pi/Nh$. The first null is at

$$\nu_{n1} = 2N/(b+a). \tag{25}$$

Since the discrete equivalent of a pill box function has $b=a+1$, the first null is at $\nu_{n1}=2N/(2a+1)$.

Thus, the essential differences between (22) and (23) is the appearance in the denominator of $(b\pm a)\sin\frac{1}{2}\theta$ instead of $(\beta\pm\alpha)\frac{1}{2}kL$, an effect called aliasing.[5] This effect causes an up-turn at the high end of the discrete spectrum. The error made in comparing $\hat{f}$ with $\hat{F}$ is

$$\epsilon = 1 - \hat{f}/\hat{F}$$

$$\epsilon = 1 - (z_+z_-)/(b^2-a^2)\left|\sin\frac{1}{2}\theta\right|^2 = 1 - \left|\frac{1}{2}\theta/\sin\frac{1}{2}\theta\right|^2. \tag{26}$$

or: 147% at $\nu = N$; 62.6% at $\nu = \frac{3N}{4}$; 23% at $\nu = \frac{1}{2}N$ and 5.3% at $\nu = \frac{1}{4}N$. The errors in the

energy spectrum, $(1 - |\hat{f}/\hat{F}|^2)$, are appreciably larger. Thus, one should be cautious about using modes beyond $\nu = 0.5N$ to estimate the exponent of power-law behavior in a numerical simulation.

B. Computational Results in Two Dimensions

For two-dimensional figures on a discrete lattice, we present "integrated" or one-dimensional energy spectra and estimated power-law exponents and amplitudes. The one-dimensional spectra have "half" the information needed to reconstruct the original discrete function, since phase information is lost through averaging.

In this section we are concerned with assessing the accuracy of spectral representations of EDF's. These are presently obtained from numerical simulations of finite-difference representations of nonlinear partial differential equations. To accomplish this, we present one-dimensional energy spectra of simple figures (like those shown in Fig. 2) and also the exponents p and amplitudes G obtained by fitting $10^{G}k^{-p}$ to the discrete spectra for various regions of k.

We will conclude by showing that p and G should be assessed with only 40% of the available modes. A quantitative assessment of: the sensitivity of errors to the fitting range; and the ability to extrapolate this exponent to higher k values are subjects requiring further study.

1. Equations

To obtain one-dimensional spectra we first take the discrete Fourier transform by using the 2D analog of (23),

$$\hat{F} = \hat{F}(k_1, k_2) = \sum \sum_{n,m=-N+1}^{n,m=N} f(nh, mh)\, e^{-i(k_1 nh + k_2 mh)}, \tag{27}$$

where we have assumed a square region with equal mesh spacings in the x and y directions and $Nh = L$. Thus, the discrete system has $(2N)^2$ independent modes in the square

$$-N + 1 \leqslant \nu_i \leqslant N, \quad (i = 1, 2), \tag{28a}$$

or

$$\frac{\pi}{h}\left(-1 + \frac{1}{N}\right) \leqslant k_i \leqslant \frac{\pi}{h} \quad (i = 1, 2). \tag{28b}$$

The one-dimensional spectra are obtained by summing over bands:

X (sum over the k_2-direction)

$$X = X(\nu_1) = \sum_{\nu_2=-N+1}^{\nu_2=+N} \hat{F}\hat{F}^*; \tag{29a}$$

Y (sum over the k_1-direction)

$$Y = Y(\nu_2) = \sum_{\nu_1=-N+1}^{\nu_1=+N} \hat{F}\hat{F}^*; \tag{29b}$$

C (sum over "circular-bands", $k = (k_1^2 + k_2^2)^{1/2} = \text{const.}$)

$$C(\nu) = \sum \hat{F}\hat{F}^* W; \tag{29c}$$

where $\nu = (\nu_1^2 + \nu_2^2)^{1/2}$, and W is a bilinear weighting factor and the sum is around circles of constant radius.[6] The circular band average is commonly used in isotropic turbulence studies as it does not favor any particular direction as do the previous two averages. It is calculated from an algorithm that "area-weights" the modes of the rectangular lattice by their closeness to circular bands on the k_1, k_2 plane. These bands are bounded by circles with radius $\nu = 1/2, 3/2, \cdots \left(N + \frac{1}{2}\right)$, and the weighted contribution in bands with radius $(2M-1)/2$ and $(2M+1)/2$ is called mode "m". The weighted contribution within the circle of radius 1/2 is designated as mode zero. Note that

$$\sum\sum_{\text{all modes}} \hat{F}\hat{F}^* = \sum_{\nu_1=-N+1}^{\nu_1=N} X(\nu_1) = \sum_{\nu_2=-N+1}^{\nu_2=N} Y(\nu_2) > \sum_{\nu=0}^{\nu=N} C(\nu). \tag{30}$$

The last inequality follows because the circular bands do not extend into farthest corners .

We have also fitted these one-dimensional spectra with the power-law function

$$H = 10^G \nu^{-p} \tag{31}$$

using a least-squares procedure over different ranges of ν. Table 1 contains summary information on the transformed figures and their one-dimensional spectra as given in Figs. 8-22. Here the amplitude $(\log_{10}X)$, $(\log_{10}Y)$ and $(\log_{10}C)$ are plotted as X, Y and O vs $\log_{10}(1+\nu)$ from $0 \leqslant \nu \leqslant N$. At the bottom of Table 1 is given the angle measured from the horizontal corresponding to exponents p.

The fitted values of p and G are designated with a $*$ or $+$ referring respectively to the 256^2 lattice or the 64^2 lattice, respectively. For the former, the mode ranges are (6-64), (25-64), (51-102) and (51-128), while for the latter the mode ranges are (1-16), (6-16), (6-25) and (12-32).

Fig. 8 shows the spectra for a pill box of radius 16 on a 256 × 256 mesh. Thus the nulls should be separated by $k\pi = \pi$ or $\nu = 8$ as the figure shows. The peaks at 14 and 22 give a straight line at 21.5° (p=2.0) and the peaks do not begin to deviate from the line until $70 < \nu < 86$. Aliasing errors qualitatively measured by "AL" in the figure arise rapidly for $\nu > 86$. The k^{+1} spectrum expected at low-k occurs at about mode 2. The exponent p that is determined in the first ν region ($6 \leqslant \nu \leqslant 64$) is accurate for C and X (2.06 and 1.99, respectively). However aliasing effects seem to occur in all the subsequent bands as seen by the monotonic decrease in p. The exponents obtained by fitting X (or Y) data do not show as strong an aliasing effect. The first band, where reliable p's are obtained, correspond to 45% of the total number of modes.

Fig. 9 shows the spectra for a 15 × 15 square ($2b_x = 2a_x = 2b_y = 2a_y = 15$) on a 256 × 256 mesh. The first null is at 17 $\left(= 1 + \frac{256}{15+1} \right)$ and the following nulls occur at every 16 mode numbers (17, 33, 49, etc.). A straight line drawn through the peaks $\nu = 25$ and 41 an angle of −21.5°, very close to $p = 2$. A straight line drawn through last two peaks has a slope of −6.2° ($k^{-0.54}$) thus showing the effect of aliasing. The height AL is due to aliasing. The band average, C, shows a k^{+1} (11.31°) behavior at mode 2. Sizeable errors begin to occur at the fourth maximum of C, mode 73, (shown by the vertical arrow). Hence, to obtain the apriori exponent ($p = 2$) we have used (100%) (73-25)/128 = 37.5% of the modes. Referring to Table 1, we see that C gives a good fit for p for $6 \leqslant \nu \leqslant 102$ but the X-fits fluctuate widely from 2.0. The C data resulting from band averaging is smoothed and p is not as sensetive to the initial and final points of the fitting interval. The highest interval gives small p's ($p = 1.32$ or 1.42) due to aliasing.

Fig. 10 shows spectra for a 31 × 31 square on a 256 × 256 mesh. The nulls are separated by 8 mode numbers. The peaks at mode 13 and 21 give an angle of −22° whereas the highest modes give an angle of −1.8° ($k^{-0.16}$). The effect of aliasing is increased at the highest modes. The p's for C-data show the monotonic decrease due to aliasing and the p's for X-data show larger fluctuations than previously, due to the sensitivity to the location of the fitting ranges.

Fig. 11 shows consistent results for a 15 × 15 square on a 64 × 64 lattice, a size typical of those used in present day numerical simulations. The nulls are spaced by 4 $\left(= \frac{64}{15+1}\right)$ mode numbers, hence a coarse sampling. If one compares with Fig. 9, one sees approximately the same percentage of modes available for determining spectral exponents. The fit to C-data in $6 \leqslant \nu \leqslant 16$ is 2.03 comparing favorably with $p = 2.0$ in C-data of Fig. 9. However, here the X-data gives a larger p (= 2.57), compared to $p = 1.62$ for Fig. 9.

Fig. 12 shows results for a trapezoidal figure, that is a 14 × 14 square with skirts ($b_x - a_x =$) 2 units wide on each side, as depicted in top view on Fig. 7c. The first two maximum (at $\nu = 25$ and $\nu = 41$) give an angle of −23.5° ($k^{-2.17}$), and the maxima at $\nu = 73$ and 89 give an angle of −38.7°(k^{-4}). The null due to the slow modulation term $\left(\sin\frac{1}{2}\,\theta(b-a)\right)$ in Eq. 23 is at $\nu = 128$ and is already evident in the more rapid fall-off at the highest modes. Thus, aliasing phenomena are suppressed. This is also evident because p falls monotonically from 2.41 to 4.71 with a value of 4.13 for $51 \leqslant \nu \leqslant 102$. Hence 40% (= 100%×(51/128)) of the modes provide a reasonable estimate of the true power law $p = 4.0$. Note the X-data yield $p = 3.87$.

Fig. 13 is also for a trapezoidal figure with skirts $(b_x - a_x) = 4$ units wide on a 24 × 24 square giving fast-modulation nulls every 16 mode numbers and the first slow-modulation null at $\left(2N/(b-a) = \right)$ 64, as indicated by the double arrow on the Fig. 13. This causes the deviation from the regular k-space oscillation apparent in the previous figures. Note, that a k^{-4} (−38.7°) region seems to be evident in the range $20 \leqslant \nu \leqslant 50$ but a k^{-2} region is not really apparent. One concludes, that a figure with skirts of 4 units on all sides of a 24 × 24 square

does not yield well-separated space scales and k-space regions are not well-separated. Thus, errors occur because of interference of slow and fast modulation terms. This is apparent when we compare p values with those obtained from the C-data of Fig. 12. The variation in p's obtained from Fig. 13 is not monotonic and in the region $51 \leqslant \nu \leqslant 102$, $p = 2.12$! In other words, because of the destructive interference, the k^{-4} spectral dependence of a corresponding continuous figure is *not* obtained by a straight-forward fitting procedure.

Fig. 14 shows results similar to Fig. 13, except that the identical figure (see Table 1) is placed on a 64×64 lattice. Thus the previous discussion applies with all mode numbers reduced by a factor of 4. Note, the non-monotonic behavior of p's with a value of $p = 4.31$ in $6 \leqslant \nu \leqslant 25$.

The next four figures (15-19) show spectra of a *rotated* rectangle with and without skirts on two different meshes. Fig. 15 is a 15×7 rectangle whose major axis is *parallel* to the x-axis. The line through the X and Y maxima is at $20°(k^{-1.8})$, whereas the line through C is at $-18.5°(k^{-1.67})$. Note the effects of aliasing. There is a "good" p behavior in $6 \leqslant \nu \leqslant 64$ and "poor" behavior in the next region. Aliasing is evident in the small values of p in $51 \leqslant \nu \leqslant 128$.

Fig. 16 shows the effect of rotating the 15×7 rectangle through 30°. All slopes shown are $-27.0°(k^{-2.6})$, that is, larger than in Fig. 15. The lower-range p values for X data (2.29 and 2.54) and Y data (2.39 and 2.27) are consistent with lines drawn on the figures. The poor estimate of $p = 1.68$ for C-data in $25 \leqslant \nu \leqslant 64$ is to do the suprising nulls at $\nu = 33$ and 63. (shown by the double arrows).

Fig. 17 shows the rotated 15×7 rectangle of the previous figure on a 64×64 mesh. The same comments apply.

Fig. 18 shows the above rotated rectangle with skirt of 2 units added to each side on a 64×64 mesh. The two lines drawn, have the same slope (angle $\simeq -36.5°$, corresponding to $k^{-3.7}$). There is no noticable k^{-2} region. The values of p in the two intermediate regions are consistent with $p = 3.7$.

The next three figures (19-21) show two 15 × 7 rectangles on a 256 × 256 mesh at varying separation along a 30° line as depicted in Fig. 7d. Fig. 19 at zero separation (corresponding to a 30 × 7 rotated rectangle) has an angle of 22.5° ($k^{-2.1}$), although there are near-plateau regions at −7° ($k^{-0.61}$). This is to be compared to the single 15 × 7 rectangle in Fig. 16 which shows larger slopes and the absence of near-plateaus. In both cases, the effect of aliasing is reduced.

For a separation of $L_s = 2$, Fig. 20, shows a larger angle, −23° (or $k^{-2.12}$) than in Fig. 17 with steep interference regions at angle of −41° ($k^{-4.35}$). Finally, on Fig. 21, for a separation of $L_s = 16$, the angle is −25.5° ($k^{-2.38}$) and again aliasing seems reduced. The fitted p values range from 2.14 to 2.37 in $6 \leqslant \nu \leqslant 64$ and anomalous values occur in the $25 \leqslant \nu \leqslant 64$ because of the interference structure observed in the figures.

To obtain Fig. 22 we have placed four rectangles on a 256 × 256 lattice as depicted in Fig. 7e (the values of the spectrum above an ordinate of 3.0 are suppressed.) The nulls and slow modulated pattern associated with single rectangles are not evident, as one expects. However, large fluctuations in Y and C are observed in the mid-range of ν and angles are about −17° ($k^{-1.53}$). The fitted p values substantiate this observation, showing values of $p < 2.02$ with values of between 1.21 and 1.66 in $51 \leqslant \nu \leqslant 128$. That is, interference effects enhance aliasing when no skirts are present.

Table 2 presents an overview of these detailed considerations. We have computed the mean and standard deviation of p in each band for C-data and X-data of the 11 different cases on a 256 × 256 lattice described in Table 1. We have done the same for the 4 different cases on a 64 × 64 lattice in the region $6 \leqslant \nu \leqslant 16$. The lowest region gives a reasonable $p \simeq 2.3$ with the smallest standard deviation of 0.4. The third region shows larger p values (2.56 for C-data and 2.58 for X-data) than the last (2.06 and 2.30). However, the last region shows large standard deviations. This undoubtedly results from the competition between aliasing (which causes the spectrum to rise) and skirts (which causes the spectrum to fall more rapidly and additionally causes slow modulation terms to appear in the spectrum). The data for 64 ×

64 lattice in $6 \leqslant \nu \leqslant 16$ seems to be dominated by the cases with skirts, for it falls closer to 4.0 and has a large standard deviation.

IV Conclusions

For EDF's with steep sides, a power law exponent of $p = 2.3$ with a standard deviation of 0.4 can be estimated from numerical simulations on a 256×256 lattice if an intermediate 40% of the modes are used. The remaining 60% of the modes are required to "*support*" the calculation. The lowest 15% of the modes are influenced by the periodic boundary conditions and the upper 45% of the modes are affected by interference effects due to skirts and errors (including numerical dissipation, dispersion and aliasing).

The 64×64 lattice does not provide enough freedom to have a large separation of space scales, that is only 13 modes ($\simeq 0.4 \times 32$) can be used to estimate p. Hence, one should treat the p's estimated on lattices of order 64×64 as tentative. However, the amplitude at the intermediate modes is probably reliable.

This conclusion suggests that a hierarchical set of numerical simulations must be made on lattices of size $\geqslant 150 \times 150$. Each run would have a different initial normalizing length. Hence the resulting spectra would apply to different regions of k-spaces thereby yielding the separation of scales necessary to obtain a trustworthy power spectrum.

More work is required to design such a hierarchy of simulation runs and to develop asymptotic techniques for matching the output of these runs.

ACKNOWLEDGMENTS

Dr. S. Sinha of the University of Pittsburgh provided figures 3 through 6. Dr. G.S. Deem provided a deck of the "CIREN" code that was used for band averaging two-dimensional Fourier spectra as described in Eq. (29c). This work was begun while NJZ was a consultant to the Naval Research Laboratory and was supported by the Defense Nuclear Agency. From 1 October 1977 he and Dr. S. Sinha were supported by the Defense Nuclear Agency and the Naval Research Laboratory through the Office of Naval Research Contract N00014-77-C-0074.

REFERENCES

1. Doles, III, J.H., N.J. Zabusky, F.W. Perkins, "Deformation and Striation of Plasma Clouds in the Ionosphere 3. Numerical Simulations of a Multilevel Model with Recombination Chemistry" J. Geophys. Res. **81**, 5987, 1976.

2. Scannapieco, A.J., S.L. Ossakow, S.R. Goldman, and J.M. Pierre, "Plasma Cloud Late Time Striation Spectra," J. Geophys. Res. **81**, 6037 1976

3. MacDonald, B.E., S.L. Ossakow, S.T. Zalesak and N.J. Zabusky "Determination of Minimum Scale Sizes in Plasma Cloud Striations," Proceedings of the Symposium, "The Effect of the Ionosphere on Space Systems and Communications," 1978.

4. Koopmans, L.H., "The Spectral Analysis of Time Series." Academic Press, 1974. Aliasing is discussed in Chapter 3.

5. Champeney, D.C. "Fourier Transforms and Their Physical Applications" New York: Academic Press, 1973. Provides good background information on continuous processes in one, two and three dimensions.

6. G.S. Deem provided CIREN, a code that computes band averages from a two-dimensional array of equispaced modes.

Table 1. Information Summary of Discrete Fourier Transformed Figures and Fitted Power-Law Exponents and Amplitude

Fig	Type	Skirt Length	2N*	Trapezoidal Figures				ν_{nx}	ν_{ny}	p for various k-ranges*				G for various k-ranges			
				$2b_x$	$2a_x$	$2b_y$	$2a_y$			*)16-64 †)1-16	25-64 6-16	51-102 6-25	51-128 12-32	*)16-64 †)1-16	25-64 6-16	51-102 6-25	51-128 12-32
8	Circle	0	256	Radius = 16				8	8	C*: 2.06 X*: 1.99	1.23 1.62	1.15 1.37	0.40 1.22	3.11 2.96	1.73 2.36	1.51 1.90	0.14 1.62
9	Square	0	256	15	15	15	15	16	16	C*: 2.13 X*: 2.21	2.0 1.62	2.1 2.86	1.32 1.42	3.08 2.65	2.88 1.71	3.11 4.01	1.67 1.38
10	Square	0	256	31	31	31	31	8	8	C*: 2.06 X*: 1.58	1.57 −0.01	1.60 1.64	1.35 1.20	3.26 1.72	2.45 −0.93	2.48 1.87	2.02 1.05
11	Square	0	64	15	15	15	15	4	4	C†: 1.54 X†: 2.87	2.03 2.57	2.22 3.32	1.17 -.39	1.97 2.00	2.42 1.89	2.60 2.58	1.31 -1.95
12	Square with skirts	2	256	18	14	18	14	16	16	C*: 2.41 X*: 2.44	2.61 2.41	4.13 3.87	4.71 4.46	3.39 3.02	3.74 3.00	6.48 5.68	7.56 6.78
13	Square with skirts	4	256	20	12	20	12	16	16	C*: 3.52 X*: 3.45	5.07 4.80	2.12 1.99	2.41 2.13	4.63 4.18	7.20 6.41	1.98 1.42	2.53 1.69
14	Square with skirts	4	64	20	12	20	12	4	4	C†: 2.60 X†: 3.27	5.02 5.08	4.31 4.26	2.75 2.54	2.41 2.65	4.86 4.54	4.15 3.75	2.18 1.60
15	Rectangle	0	256	15	15	7	7	16	32	C*: 2.00 X*: 2.21 Y*: 2.46	1.31 1.65 0.01	2.43 2.80 3.13	1.16 1.42 0.94	2.81 2.36 3.14	1.64 1.47 -0.96	3.59 3.61 4.45	1.28 1.09 0.45
16	Rectangle at 30°	0	256	15	15	7	7	16	32	C*: 2.17 X*: 2.29 Y*: 2.39	1.68 2.54 2.27	3.47 3.35 2.00	2.66 3.33 2.34	3.00 2.98 3.16	2.15 3.38 2.95	5.28 4.81 2.40	3.82 4.77 3.00
17	Rectangle at 30°	0	64	15	15	7	7	4	8	C†: 1.24 X†: 2.11 Y†: 2.06	2.23 2.58 2.74	2.68 2.91 2.65	2.94 3.40 2.84	1.52 2.12 2.10	2.45 2.57 2.75	2.88 2.89 2.67	3.28 3.51 2.92
18	Rectangle at 30° in skirts	2	64	19	15	11	7	3.76	7.11	C†: 1.67 X†: 2.61 Y†: 2.38	3.23 3.74 3.03	3.55 4.11 3.94	5.12 4.82 4.64	1.81 2.39 2.29	3.33 3.52 2.90	3.66 3.88 3.79	5.63 4.76 4.65
19	Two rectangles both at 30° separation = 0	0	256	15	15	7	7	16	32	C*: 2.30 X*: 2.25 Y*: 2.38	1.51 2.32 1.91	3.14 2.84 1.94	2.32 2.87 2.50	3.42 3.15 3.45	2.07 3.27 2.64	4.97 4.21 2.61	3.46 4.26 3.63
20	Two rectangles both at 30°, separation = 2	0	256	15	15	7	7	16	32	C*: 2.14 X*: 2.23 Y*: 2.36	1.26 2.30 1.88	3.27 2.84 1.93	2.31 2.81 2.49	3.20 3.11 3.39	1.72 3.22 2.58	5.21 4.20 2.58	3.45 4.13 3.60
21	Two rectangles both at 30°, separation = 16	0	256	15	15	7	7	16	32	C*: 2.14 X*: 2.30 Y*: 2.37	1.72 2.55 2.23	3.19 3.25 1.98	2.53 3.24 2.40	3.25 3.28 3.44	2.51 3.70 3.19	5.08 4.92 2.67	3.88 4.92 3.44
22	Four rectangles	0	256	–	–	–	–	–	–	C*: 1.85 X*: 2.00 Y*: 1.78	1.81 1.69 2.02	1.54 1.56 1.82	1.57 1.21 1.66	4.14 3.75 3.87	4.33 3.23 4.28	3.63 2.98 3.96	3.67 2.34 3.66

*p values corresponding to angles of lines drawn on Figs. 8-22.

-(angle)°	5.71°	11.31	16.70	21.80	26.57	30.96	35.0	38.66	45.0	50.19
p	0.5	1.0	1.5	2.0	2.5	3.0	3.5	4.0	4.5	5.0

Table 2 – OVERVIEW: Mean and Standard Deviation of p Exponents

	DATA	CASES	$(2N)^2 = 256^2$ RANGE of ν				$(2N)^2 = 64^2$ RANGE of ν	
			6-64	25-64	51-102	51-128	CASES	6-16
MEAN	C	11	2.25	1.98	2.56	2.06	4	3.13
	X	11	2.26	2.13	2.58	2.30	4	3.49
STD.DEV	C	11	0.42	1.1	0.90	1.1	4	1.18
	X	11	0.43	1.1	0.78	1.1	4	1.03

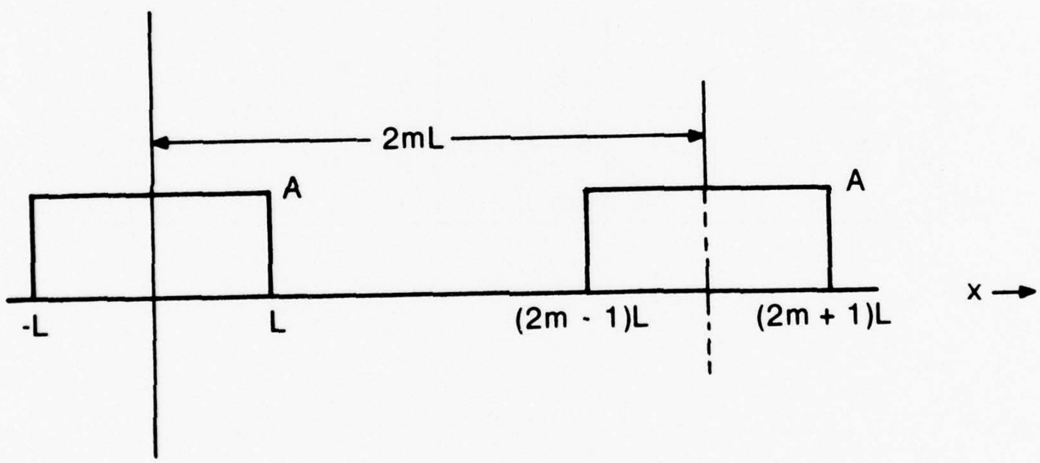

Fig. 1 — Two rectangular figures in one dimension

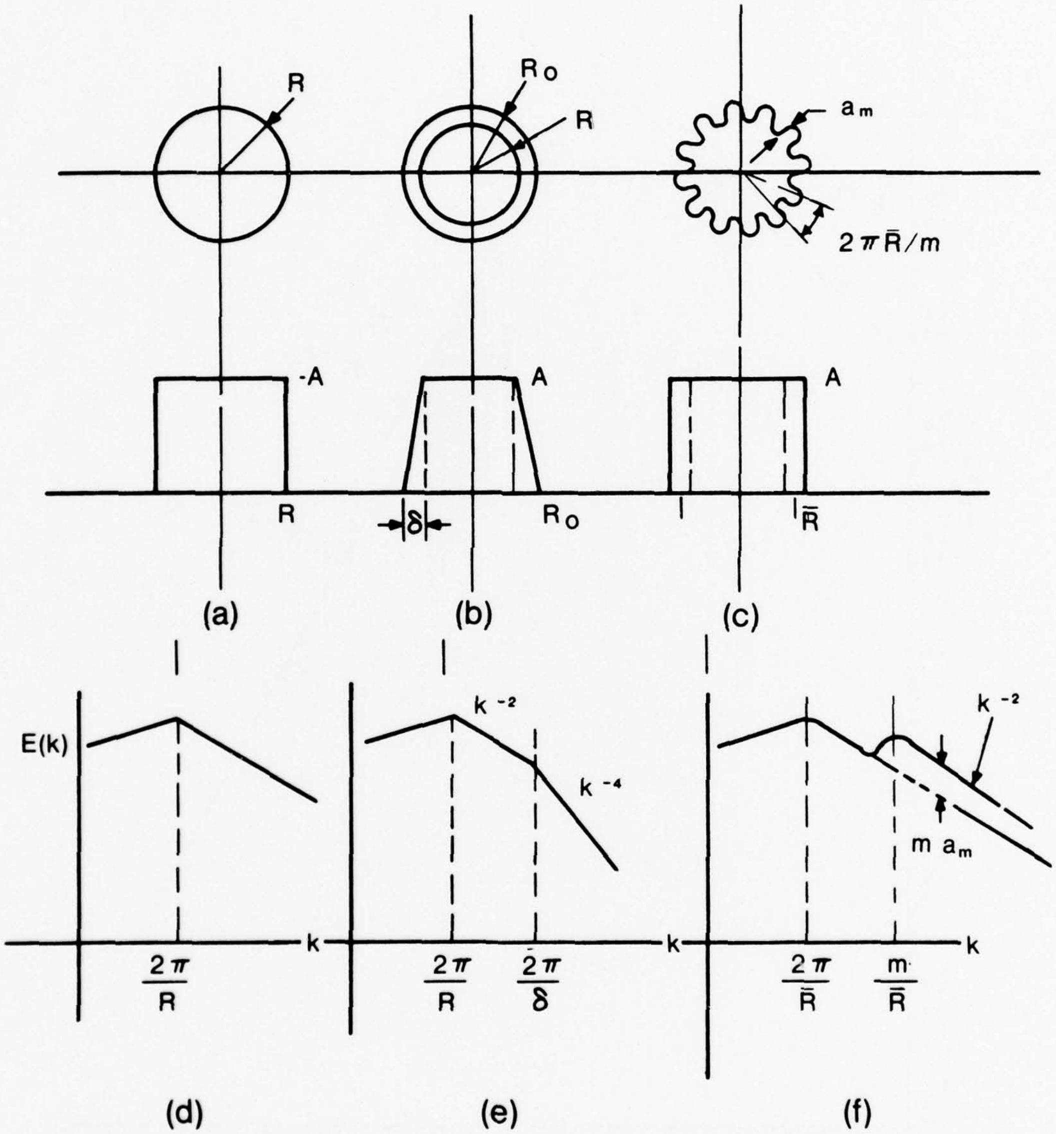

Fig. 2 — Figures with azimuthal symmetry (a,b,c) and schematic of their one-dimensional energy spectra (d,e,f). (a,d) Pill-box or cylinder, f_P; (b,e) Frustum of a cone, f_F; (c,f) Pill-box with azimuthal modulation at wave number m.

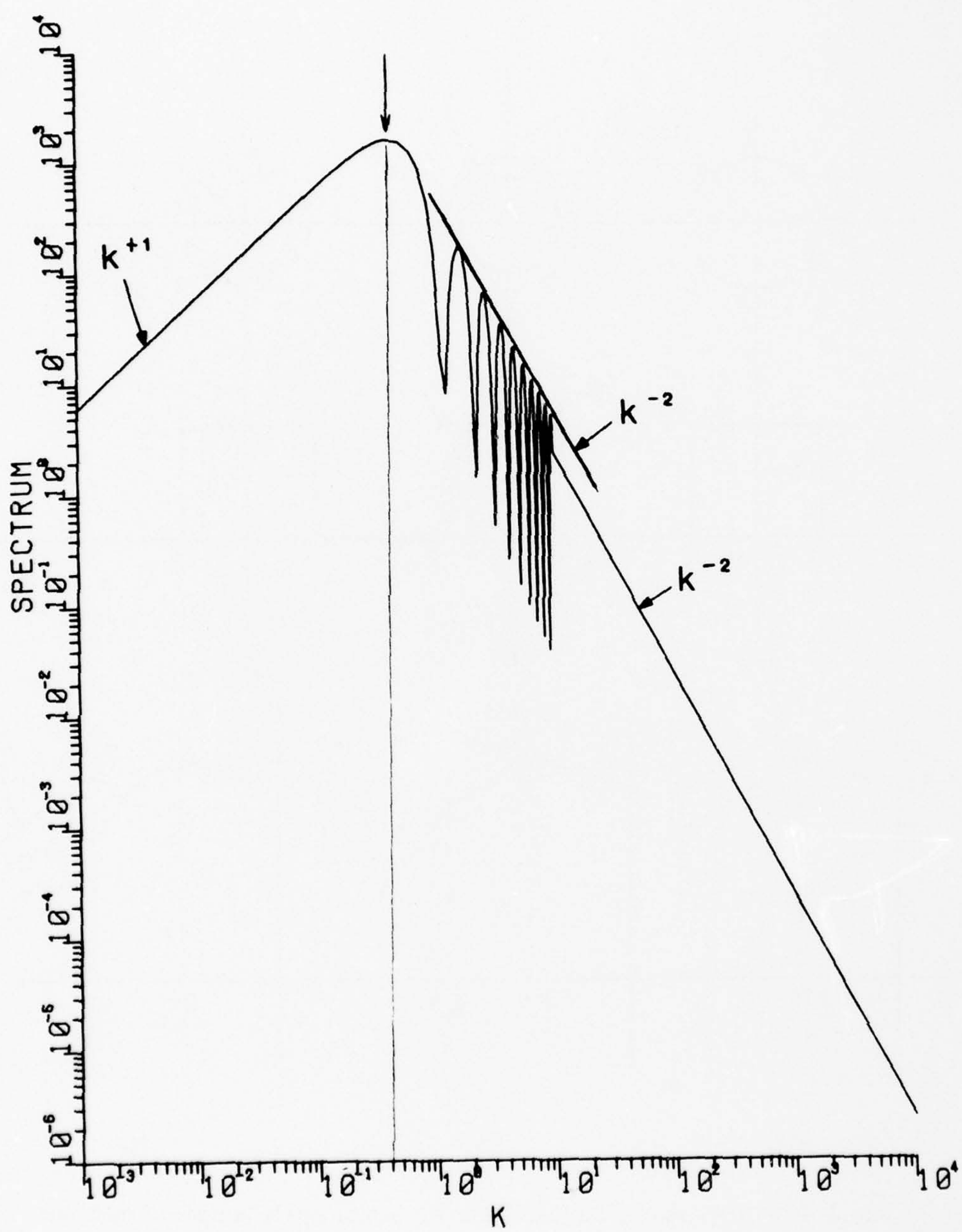

Fig. 3 — One-dimensional energy spectrum for a single pill box of radius $R = \pi, A = 1$.

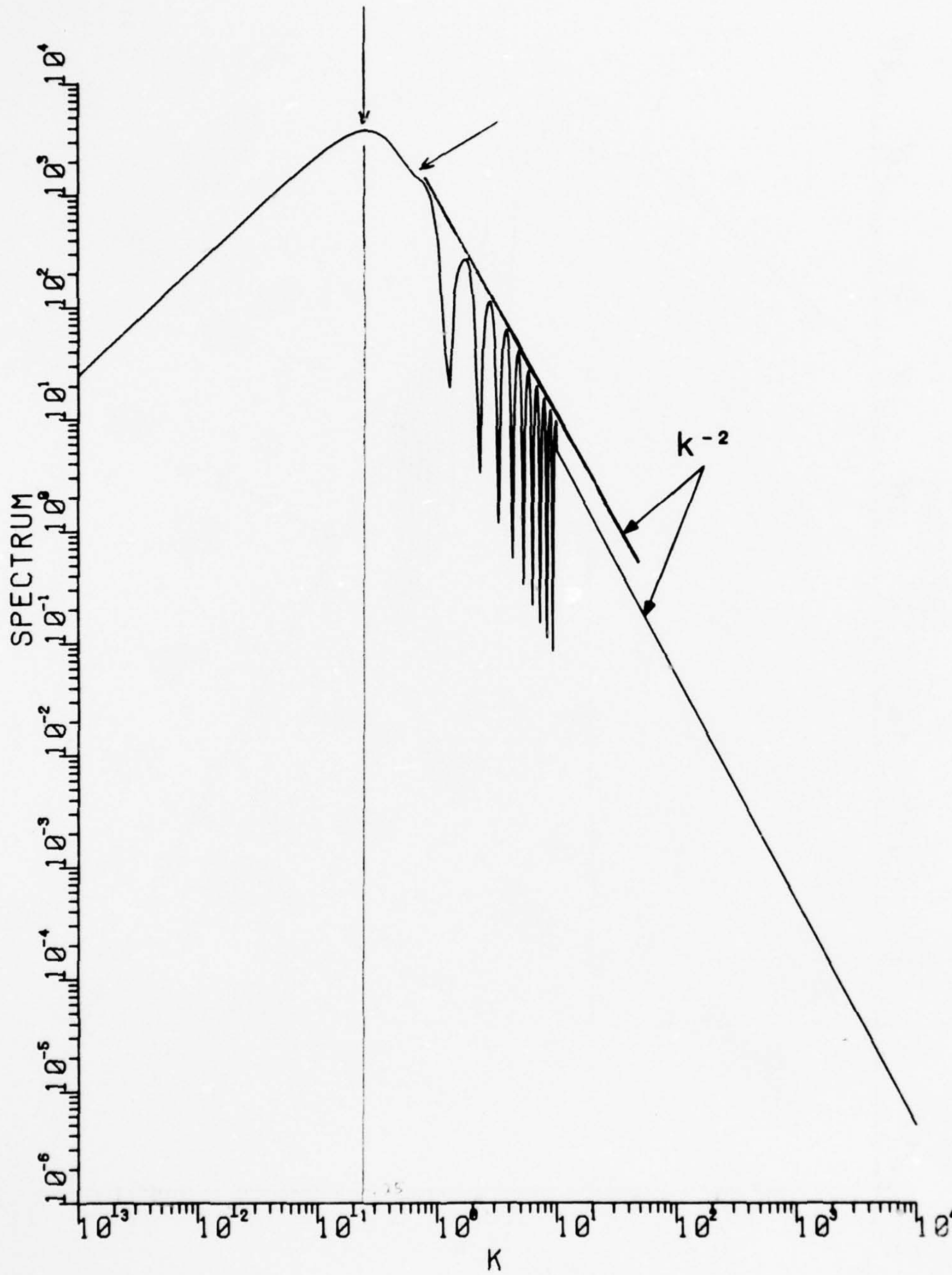

a) $r_{12} = 2\pi$;

Fig. 4 — One-dimensional energy spectrum for two pill boxes, each of $R = \pi$ and $A = 1$. Distance between centers:

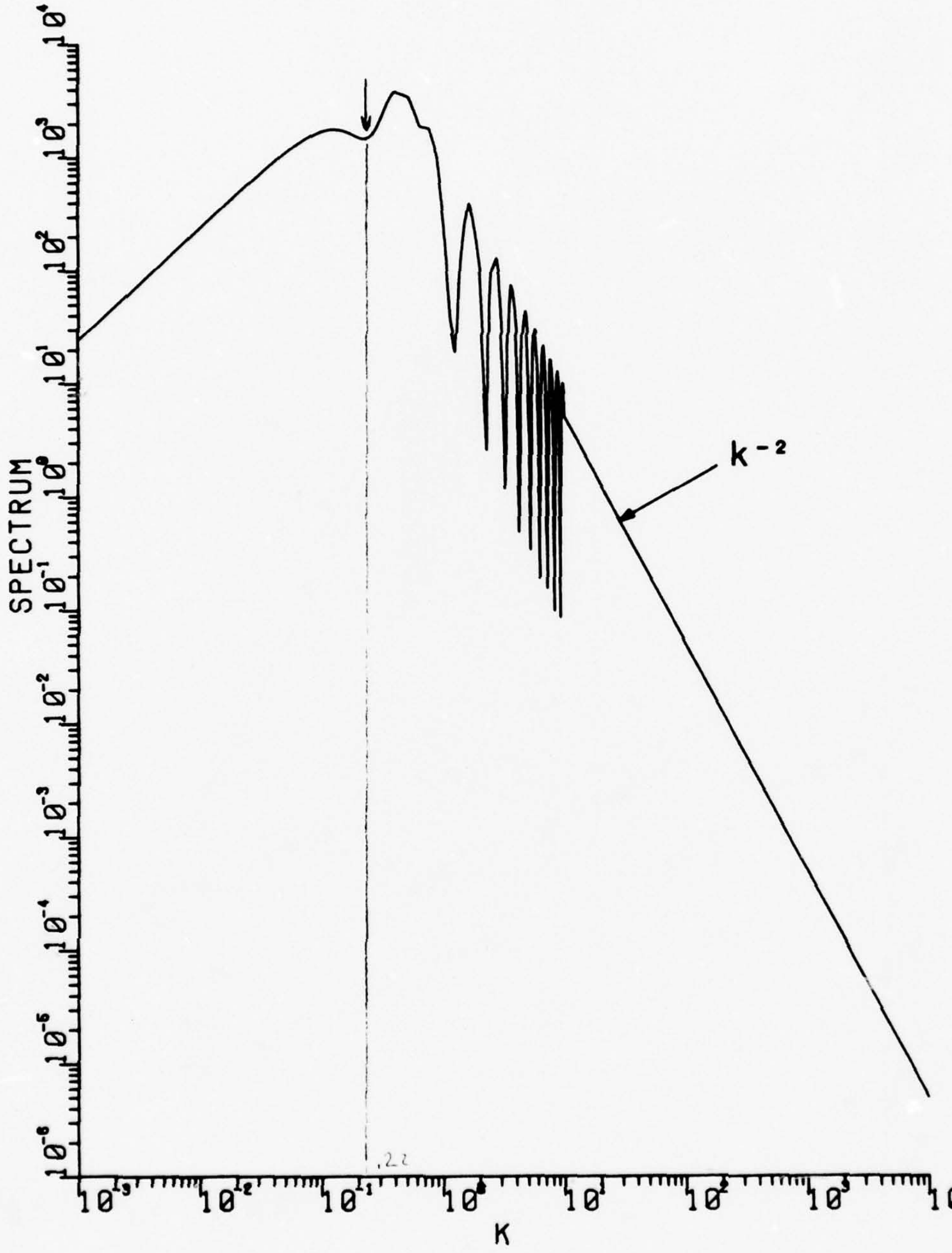

b) $r_{12} = 5\pi$;

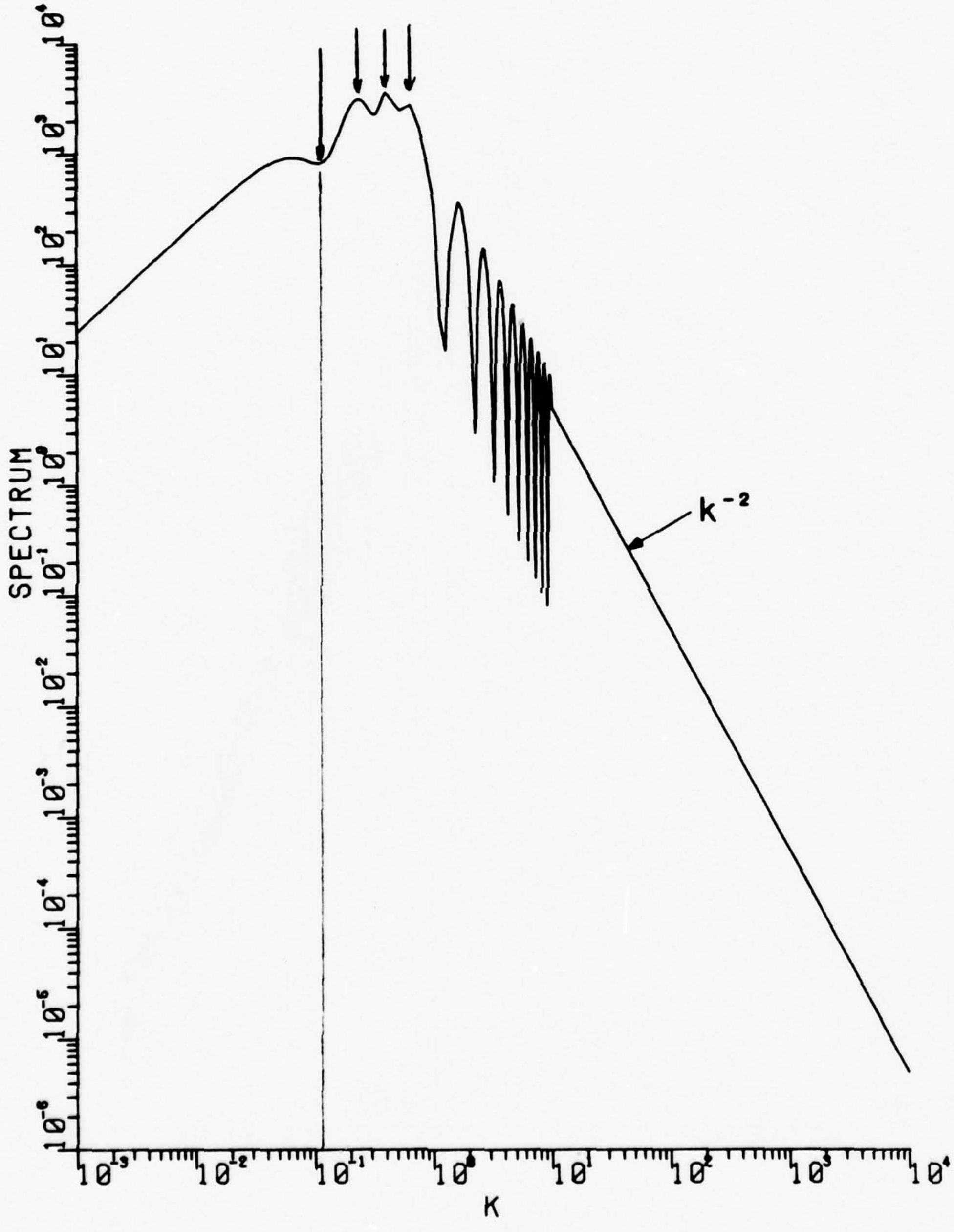

c) $r_{12} = 10\pi$.

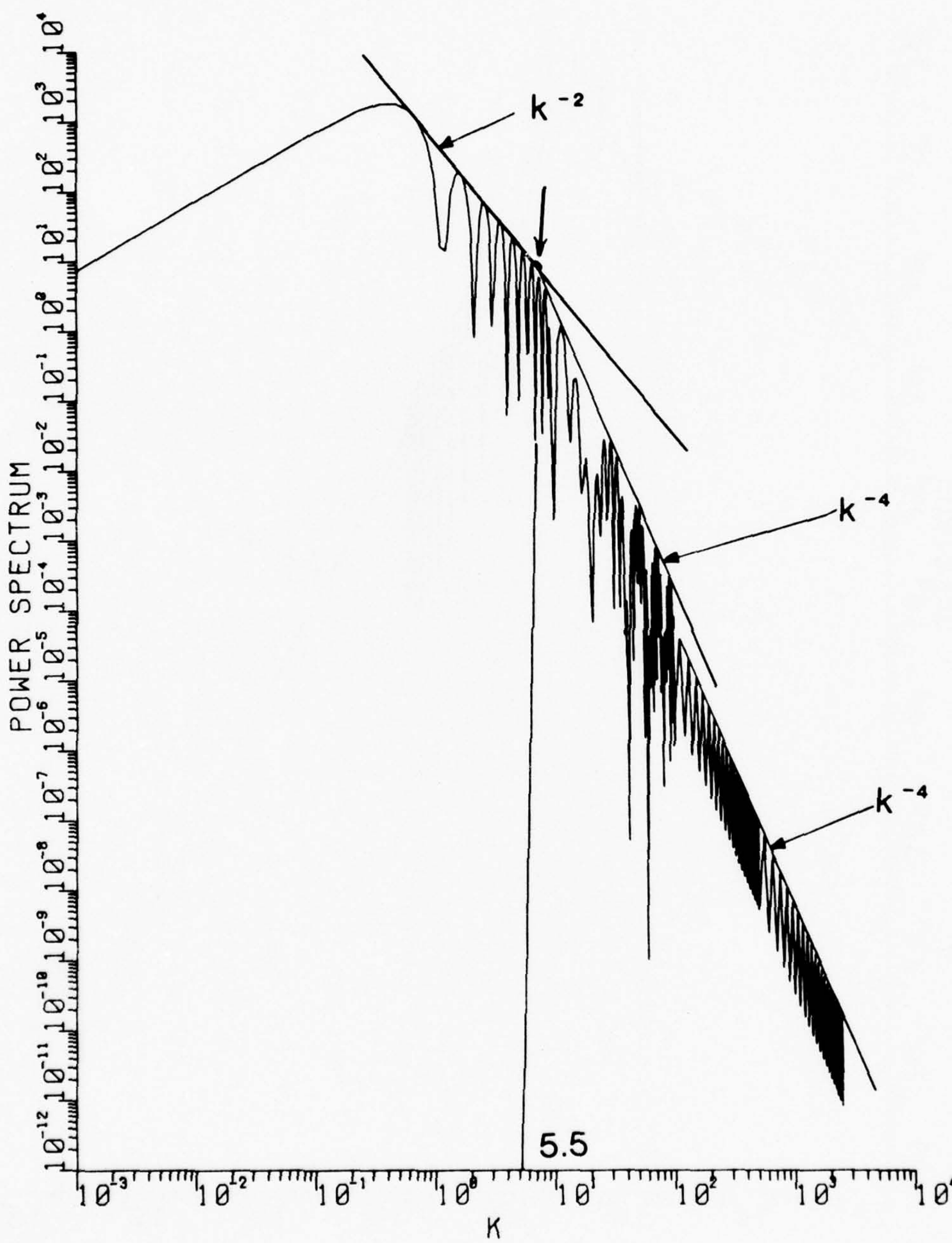

a) $R_o = 1.1\pi$;

Fig. 5 — One-dimensional energy spectrum for a frustum of a cone with $A = 1$ and $R = \pi$.

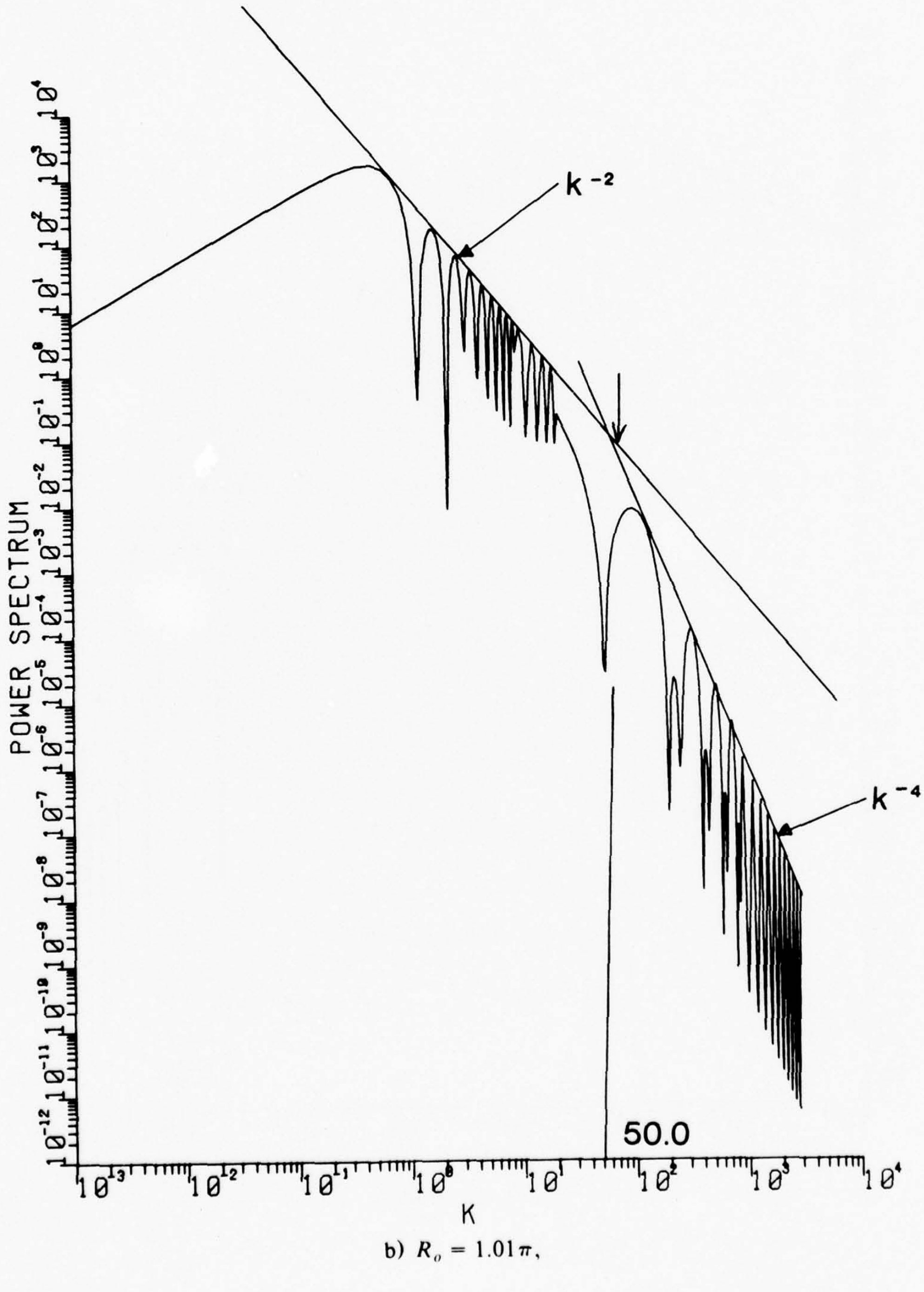

b) $R_o = 1.01\pi$,

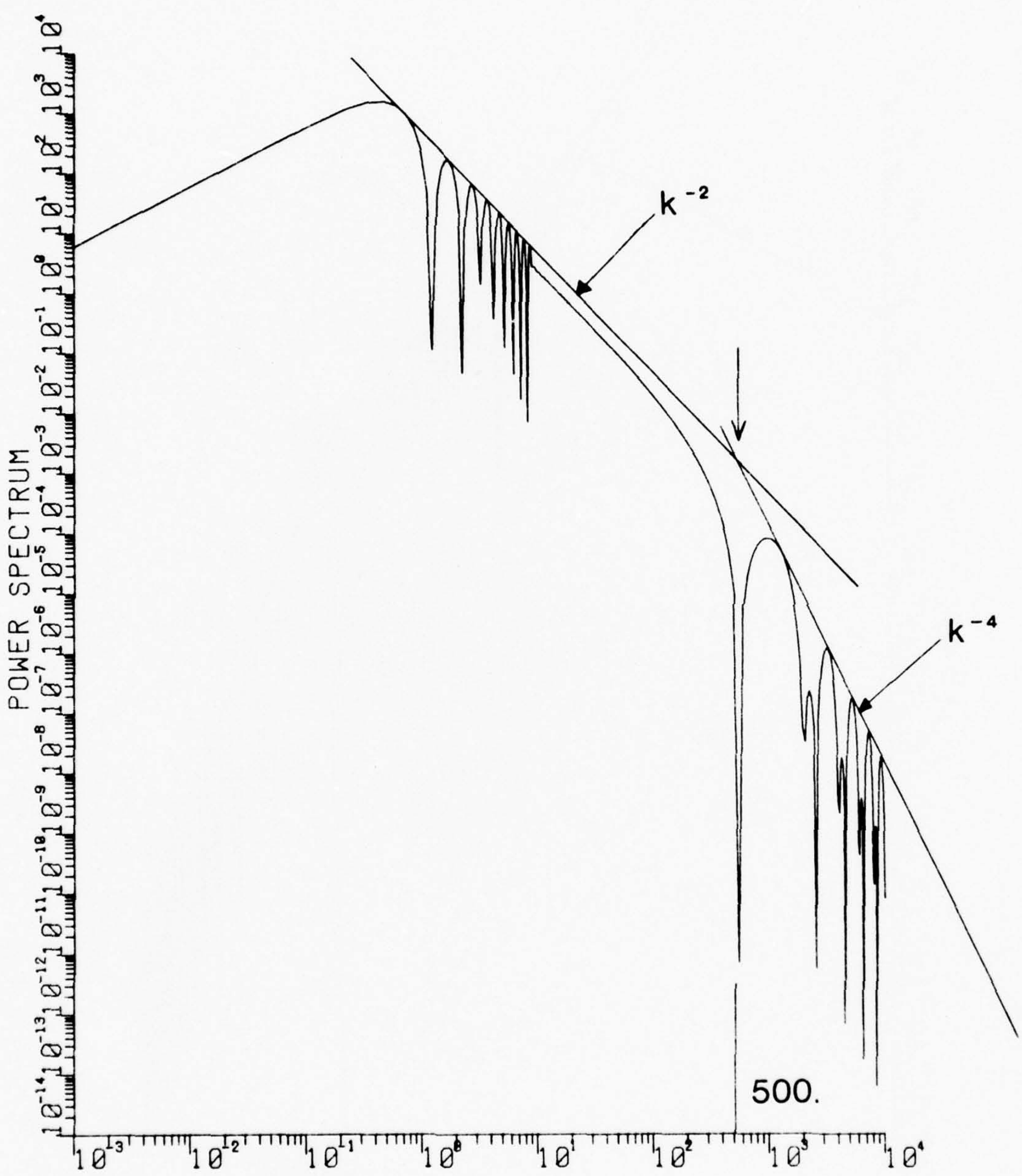

c) $R_o = 1.001\pi$

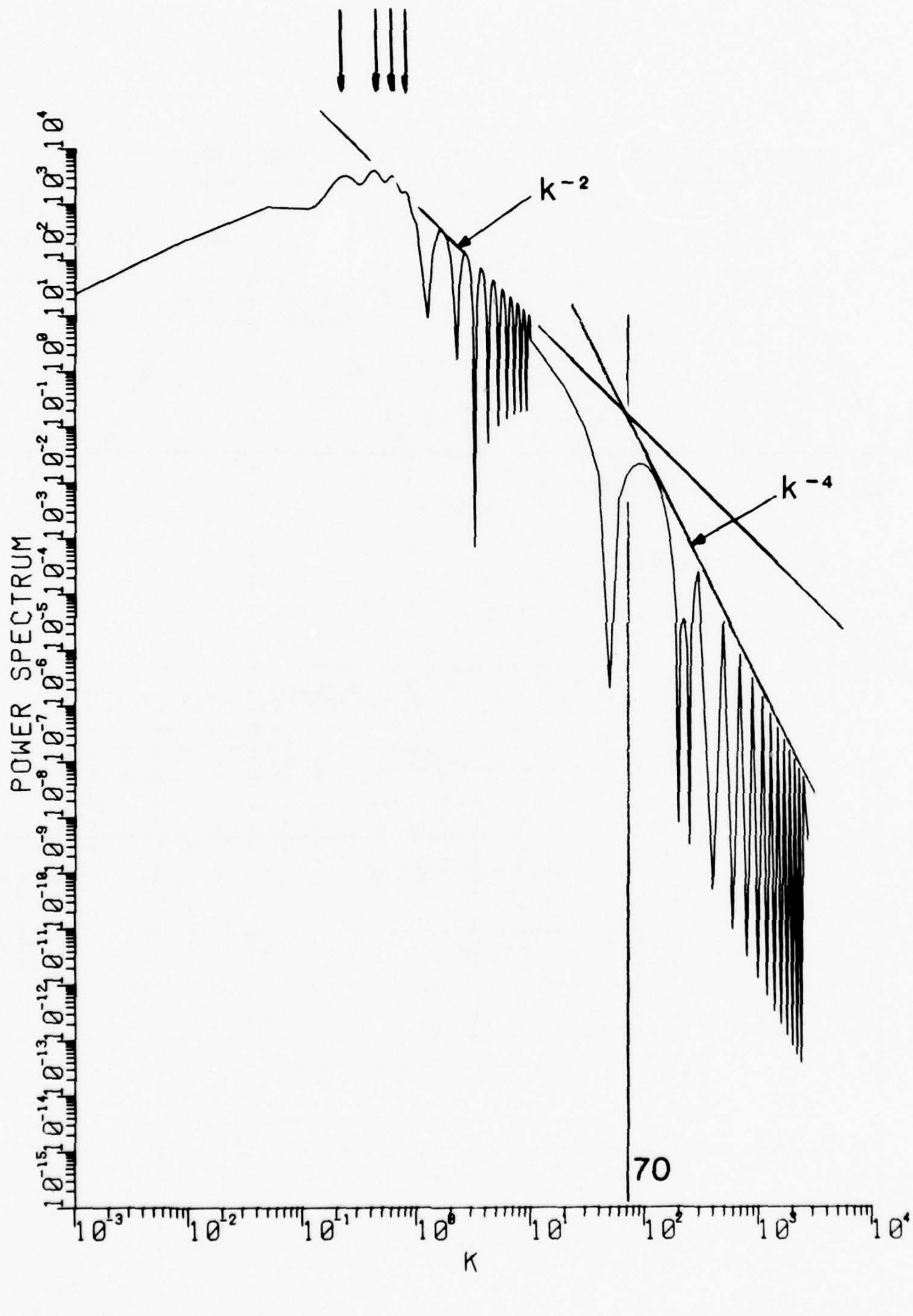

POWER SPECTRUM OF TWO FRUSTUMS,RS=(1.01)R,(10)R APART,R=PI

Fig. 6 — One-dimensional energy spectrum for two frustums of cones. $A = 1$, $R = \pi$, $R_o = 1.01\pi$ and $r_{12} = 10\pi$.

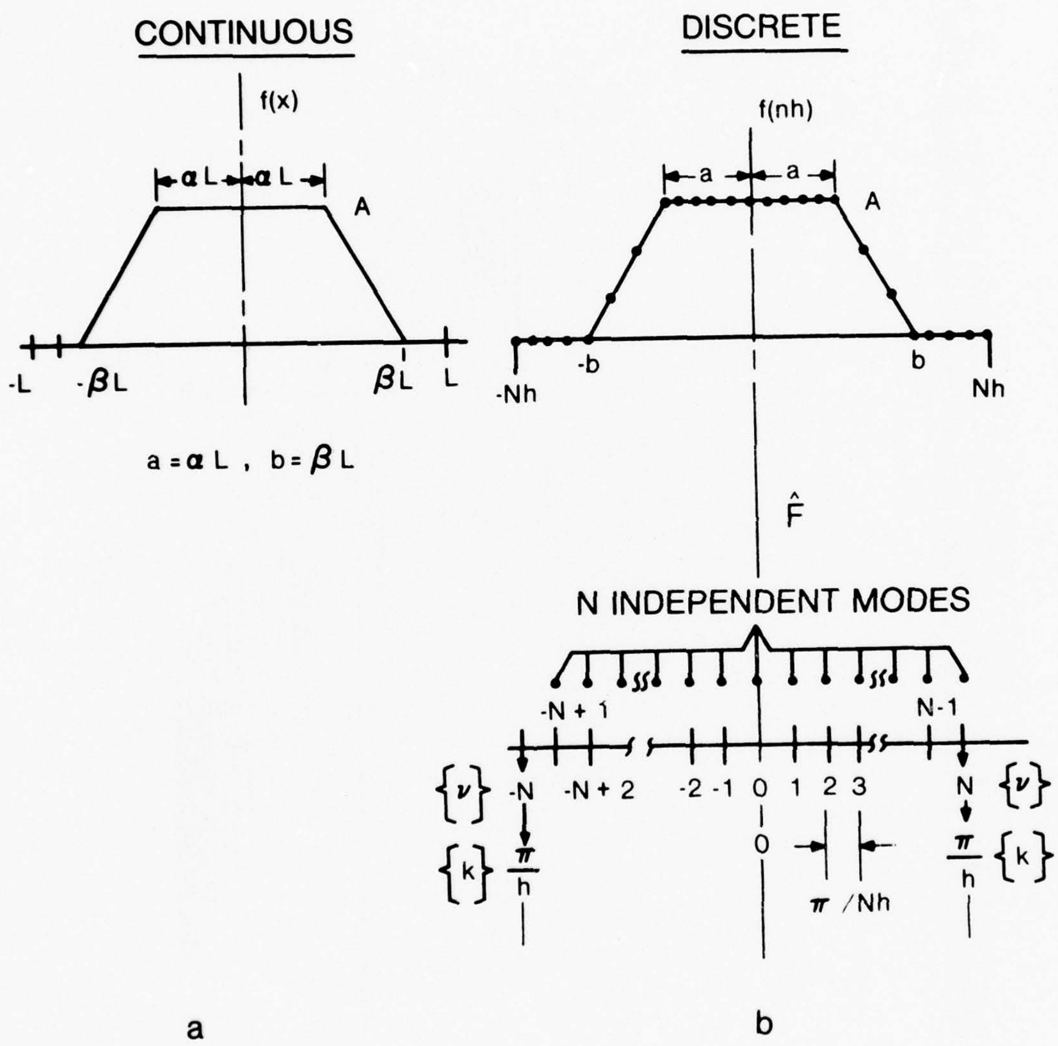

Fig. 7 — Schematics for continuous and discrete Fourier transforms in one and two dimensions.

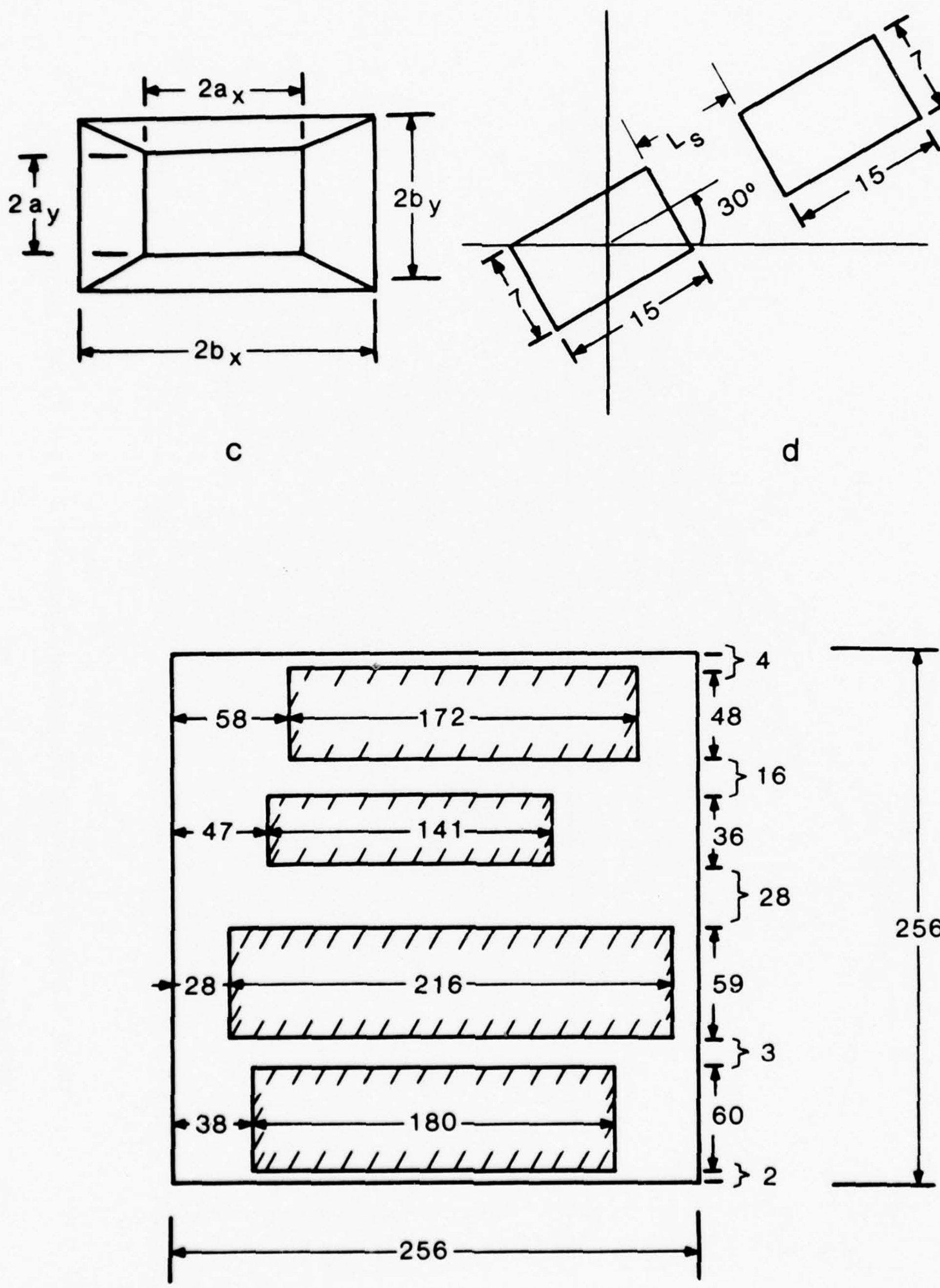

e

Fig. 7 – Schematics for continuous and discrete Fourier transforms in one and two dimensions.

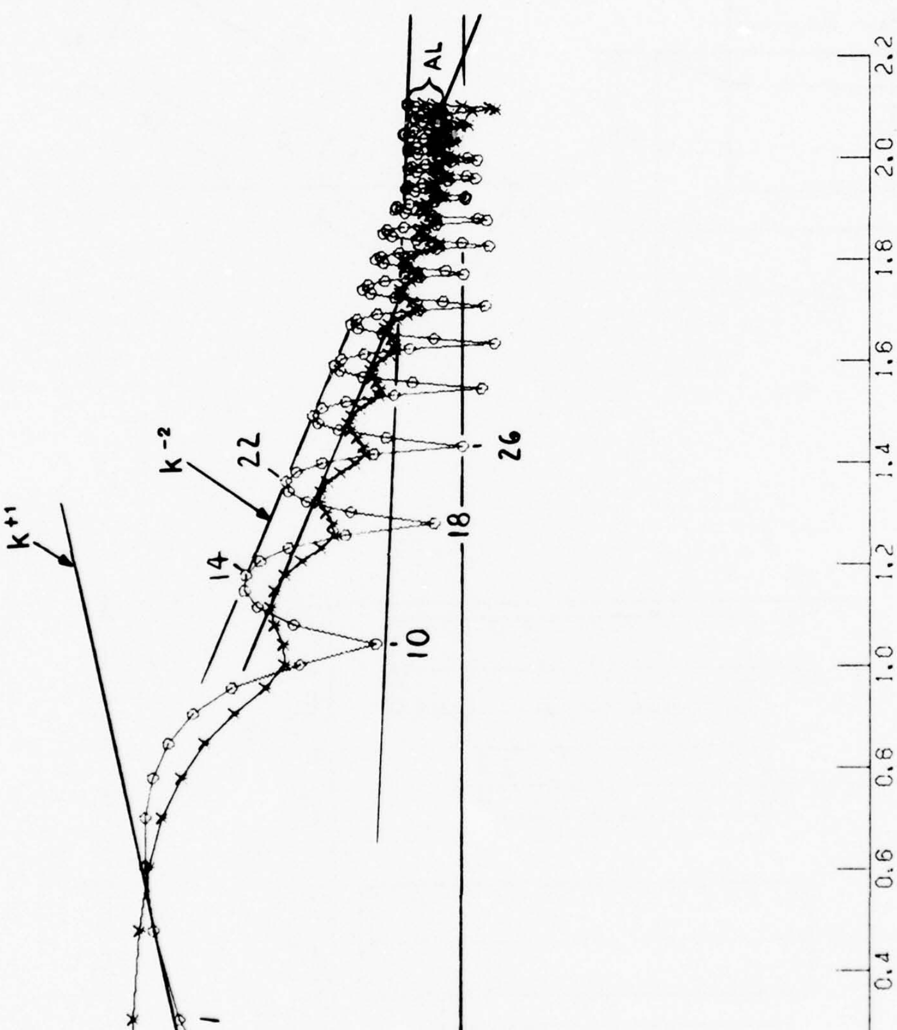

Fig. 8 — Discrete one-dimensional energy spectra ($X = Y$ and O) for a circular pill box. $A = 1$, $R = 16$ and $(2N)^2 = 256^2$.

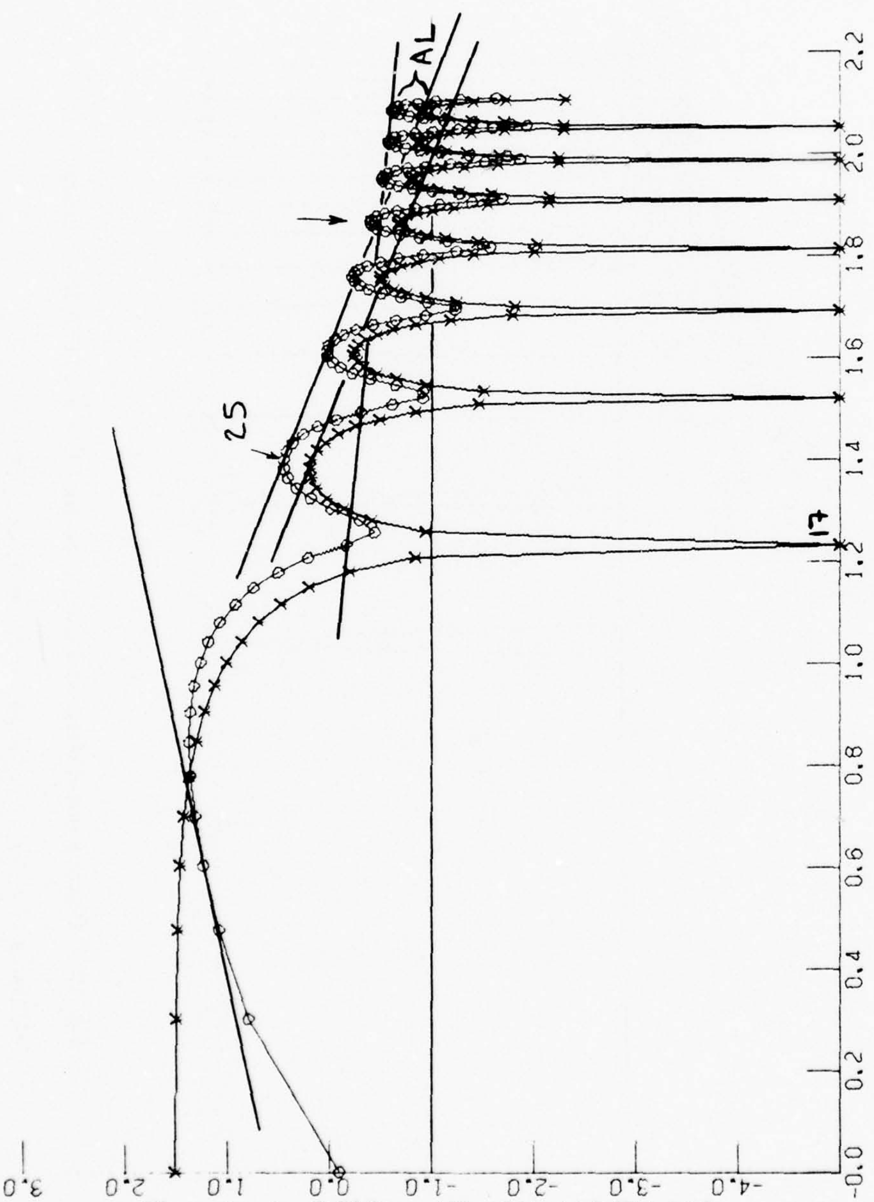

Fig. 9 — Discrete one-dimensional energy spectra ($X = Y$ and O) for a square pill-box. $A = 1$, $2a_x = 2a_y = 2b_x = 2b_y = 15$ and $(2N)^2 = 256^2$.

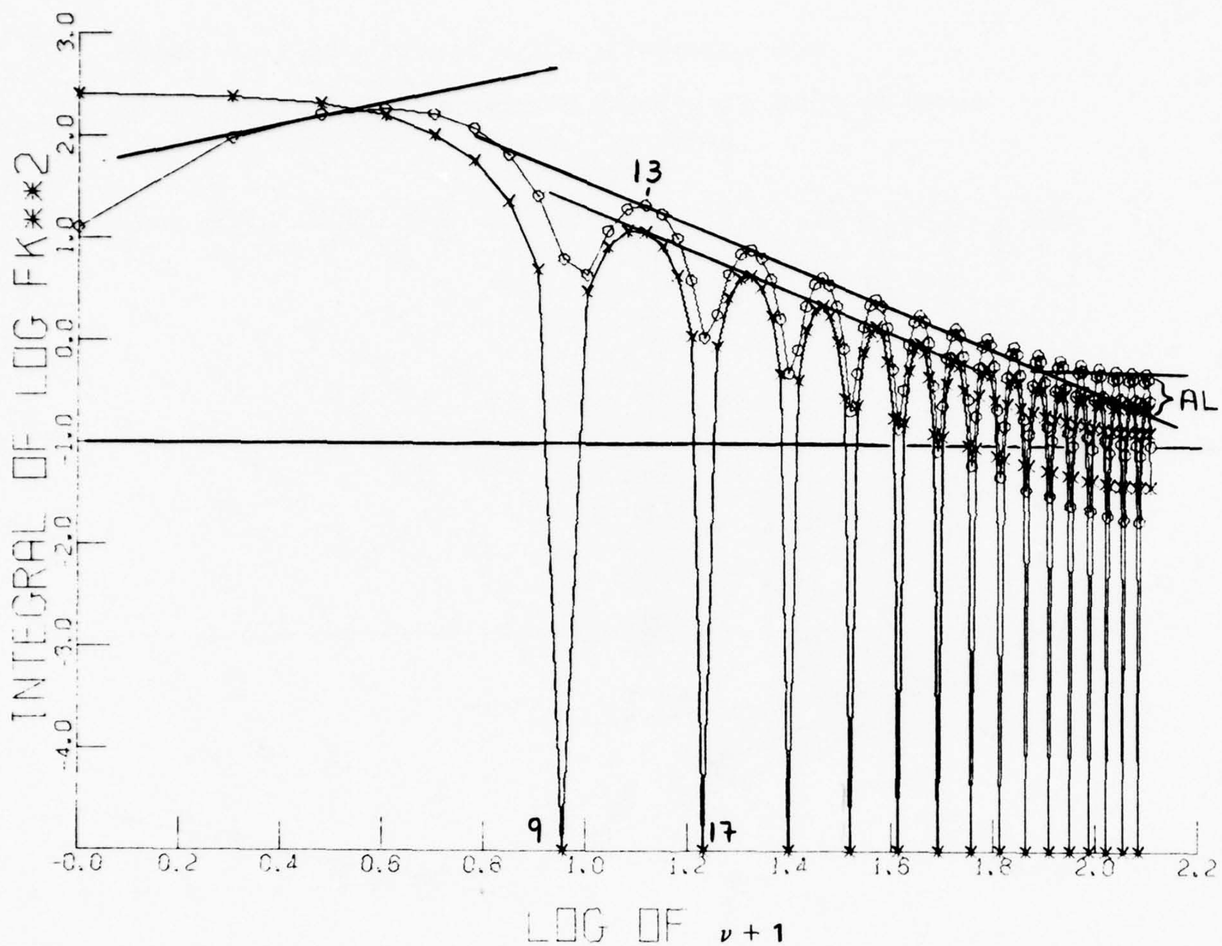

Fig. 10 — Discrete one-dimensional energy spectra ($X = Y$ and O) for a square pill-box $A = 1$, $2a_x = 2a_y = 2b_x = 2b_y = 31$ and $(2N)^2 = 256^2$.

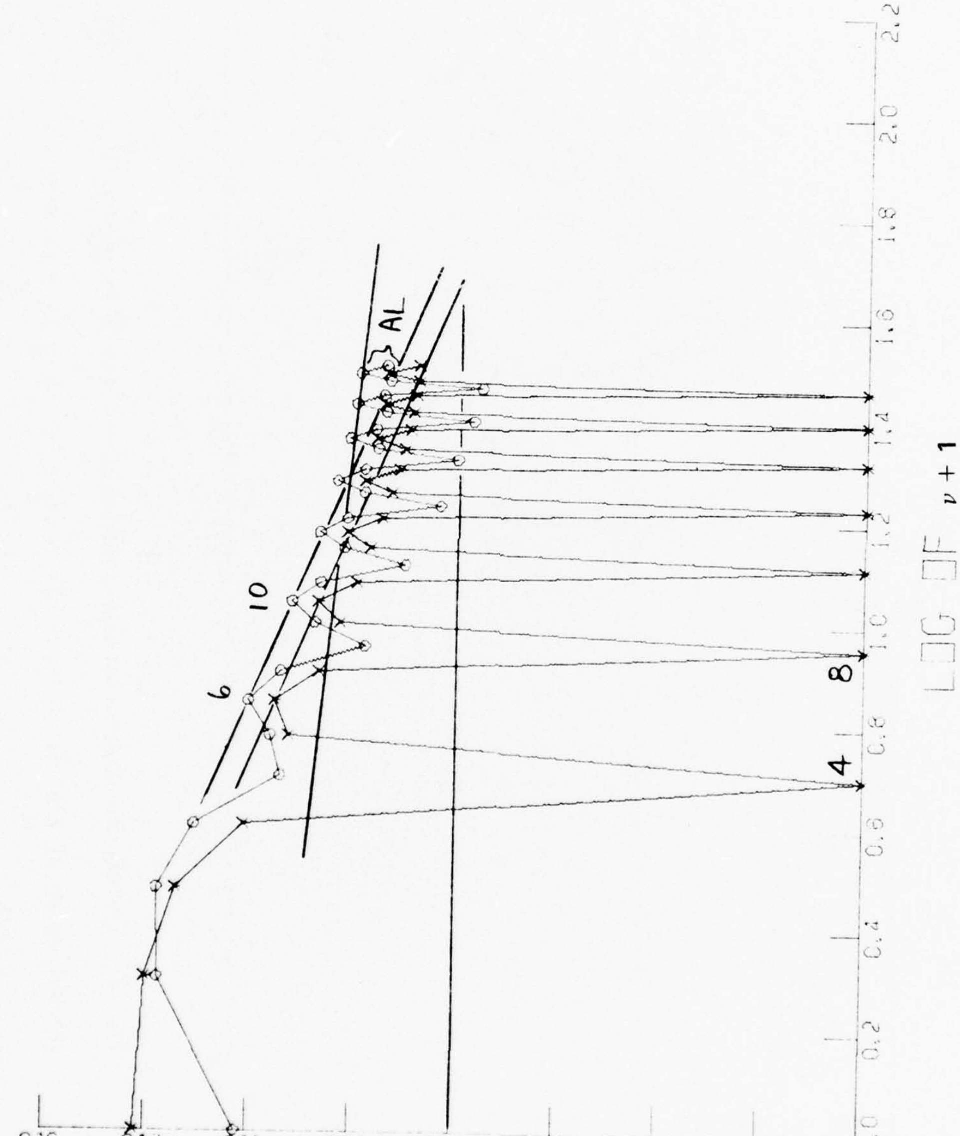

Fig. 11 — Discrete one-dimensional energy spectra ($X = Y$ and O) for a square pill box. $A = 1$, $2a_x = 2a_y = 2b_x = 2b_y = 15$ and $(2N)^2 = 64^2$.

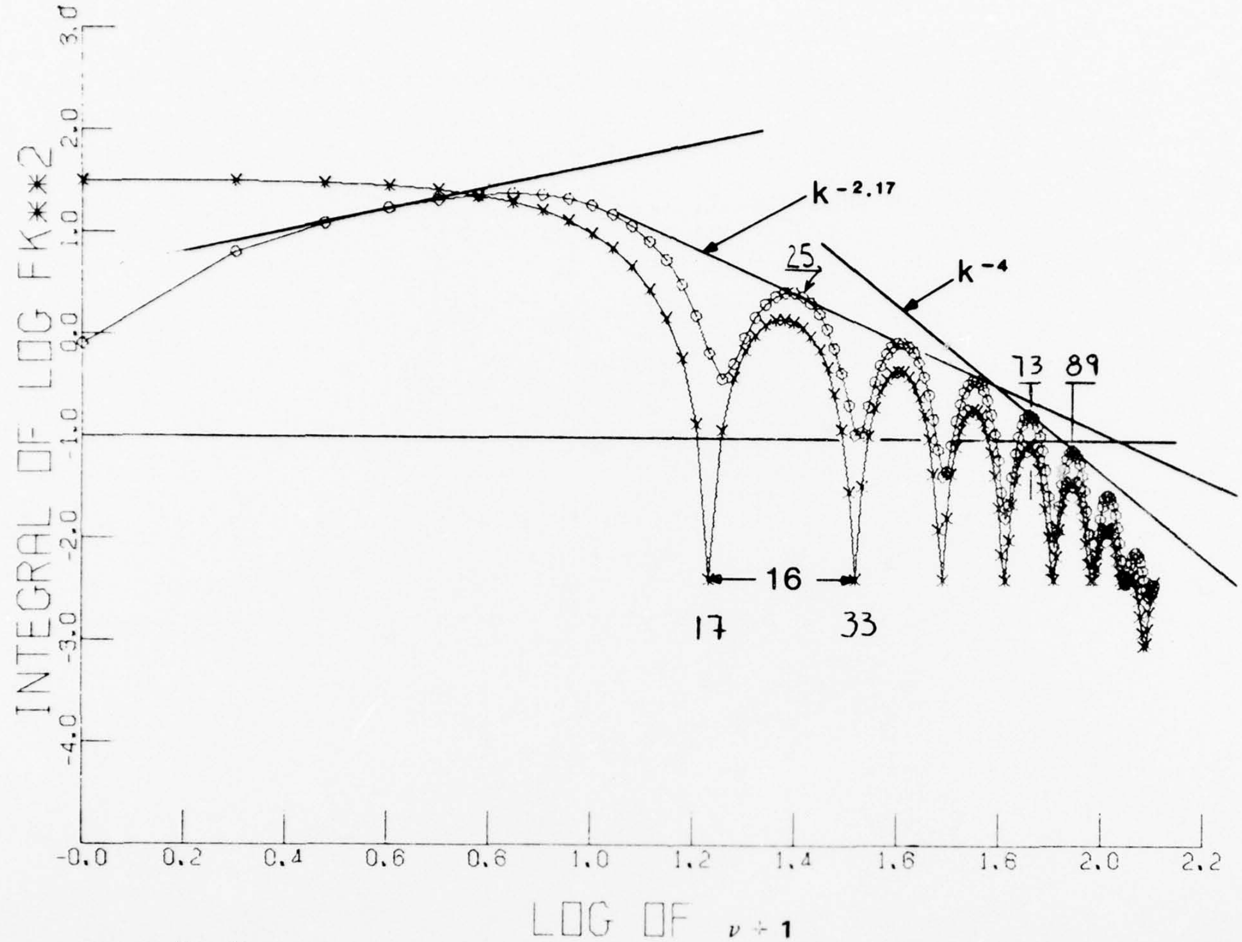

Fig. 12 — Discrete one-dimensional energy spectra ($X = Y$ and O) for the trapezoidal figure of Fig. 7c. $A = 1$, $2a_x = 2a_y = 14$, $2b_x = 2b_y = 18$ and $(2N)^2 = 256^2$.

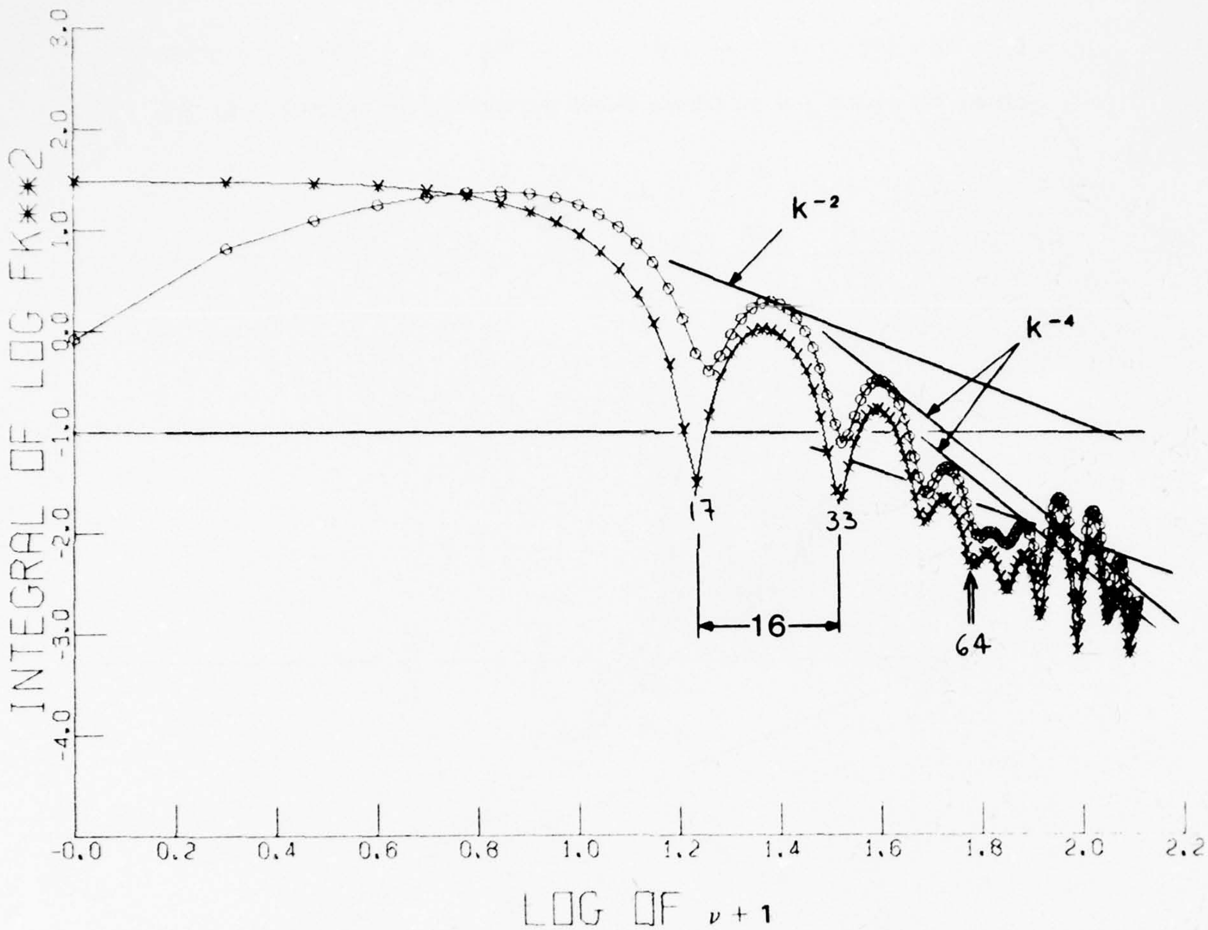

Fig. 13 — Discrete one-dimensional energy spectra ($X = Y$ and O) for the trapezoidal figure of Fig. 7c. $A = 1$, $2a_x = 2a_y = 12$, $2b_x = 2b_y = 20$, and $(2N)^2 = 256^2$.

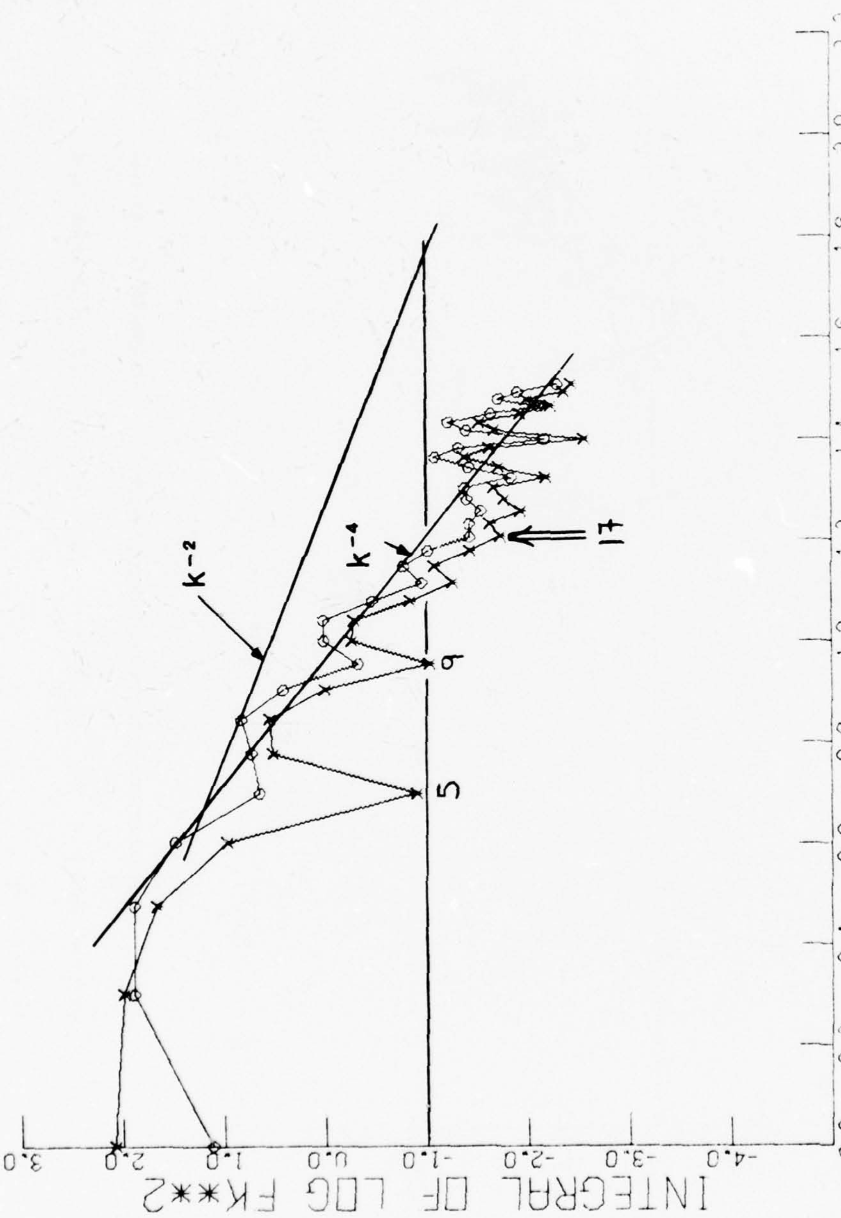

Fig. 14 — Discrete one-dimensional energy spectra ($X = Y$ and O) for the trapezoidal figure of Fig. 7c. $A = 1$, $2a_x = 2a_y = 12$, $2b_x = 2b_y = 20$, and $(2N)^2 = 64^2$.

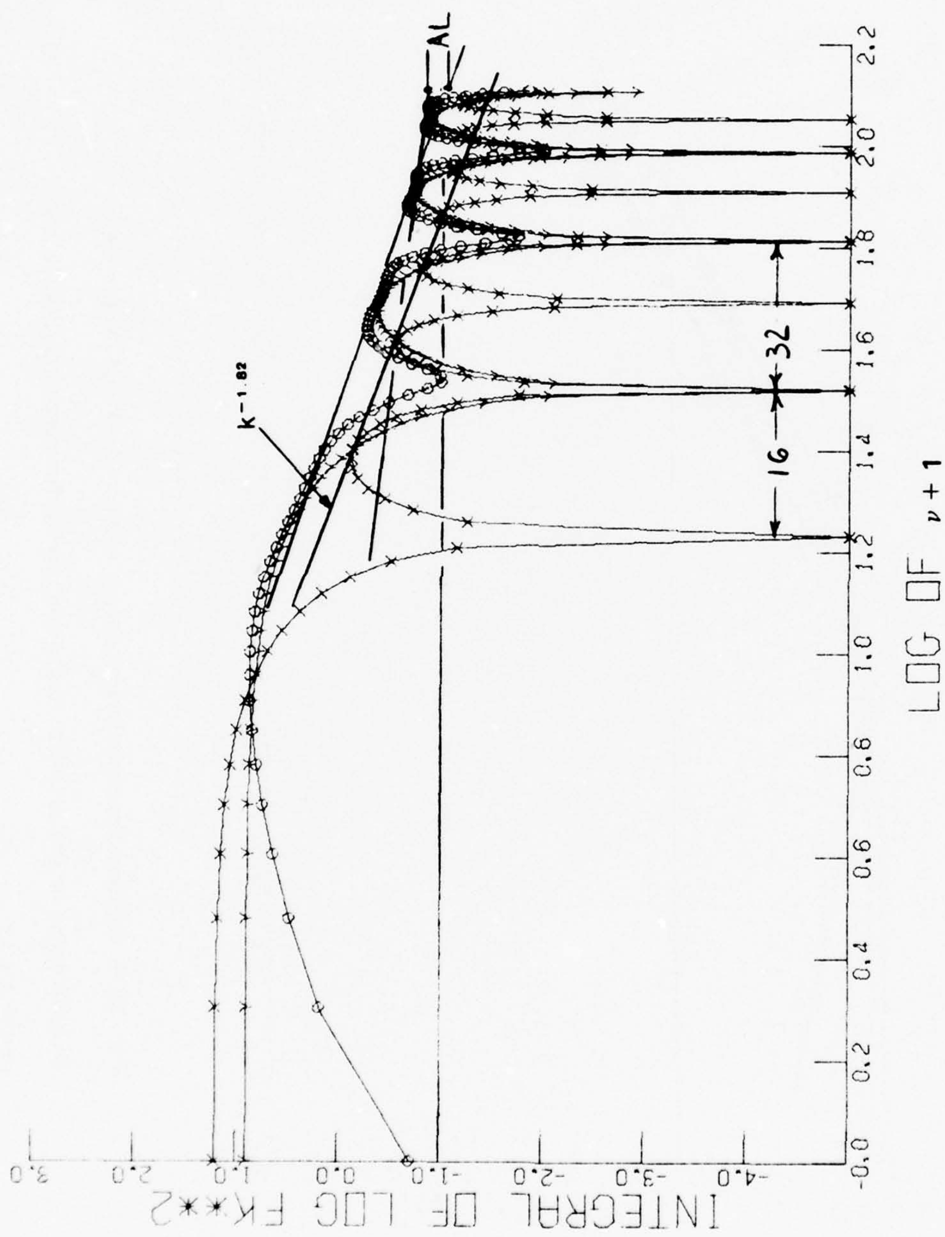

Fig. 15 — Discrete one-dimensional energy spectra. ($X = Y$ and O) for a *rectangular* figure of Fig. 7c. $A = 1$; $2a_x = 2b_x = 15$; $2a_y = 2b_y = 7$ and $(2N)^2 = 256^2$.

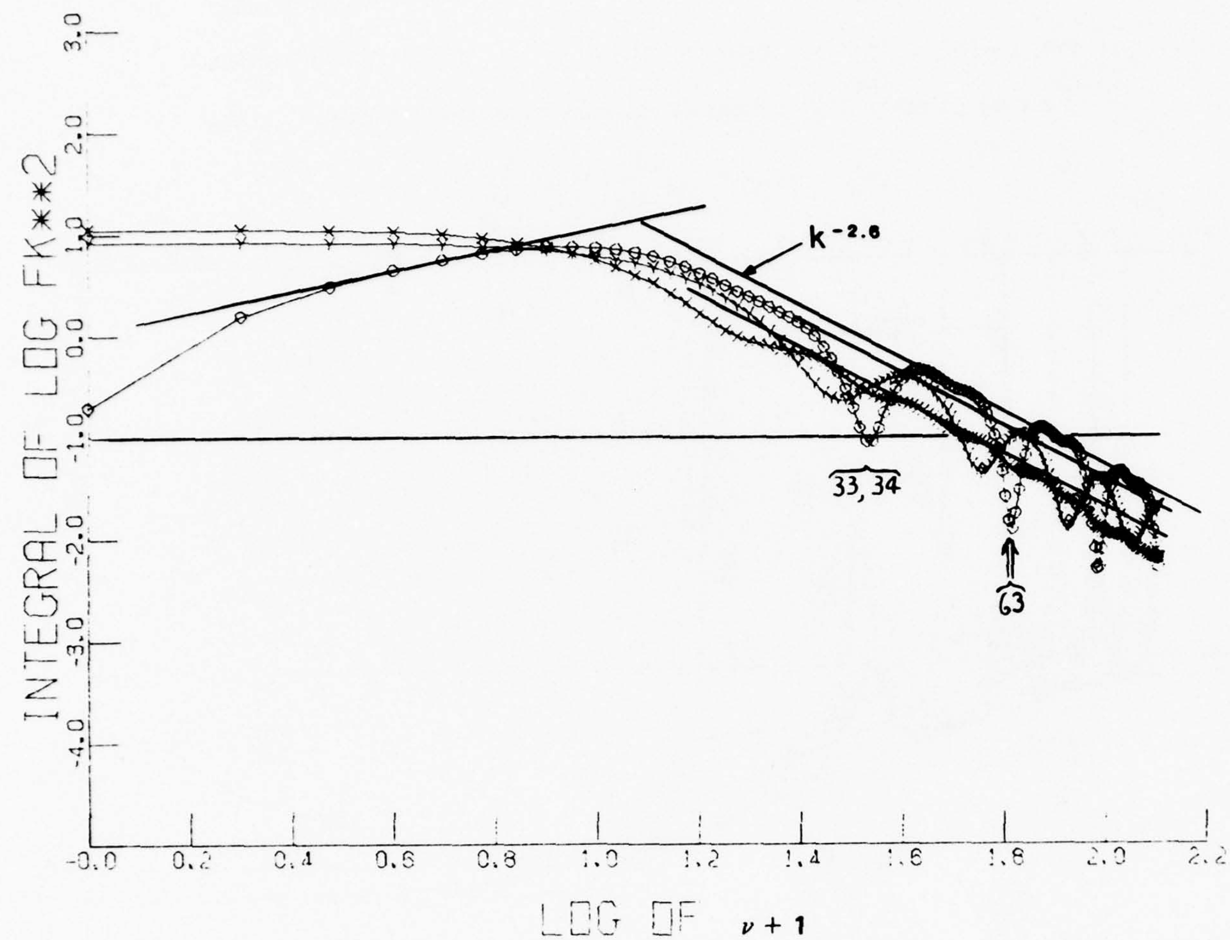

Fig. 16 — Discrete one-dimensional energy spectra (X, Y and O) for a *rectangular* figure *rotated* at 30° to the x-axis. Same dimensions as Fig. 15 and $(2N)^2 = 256^2$.

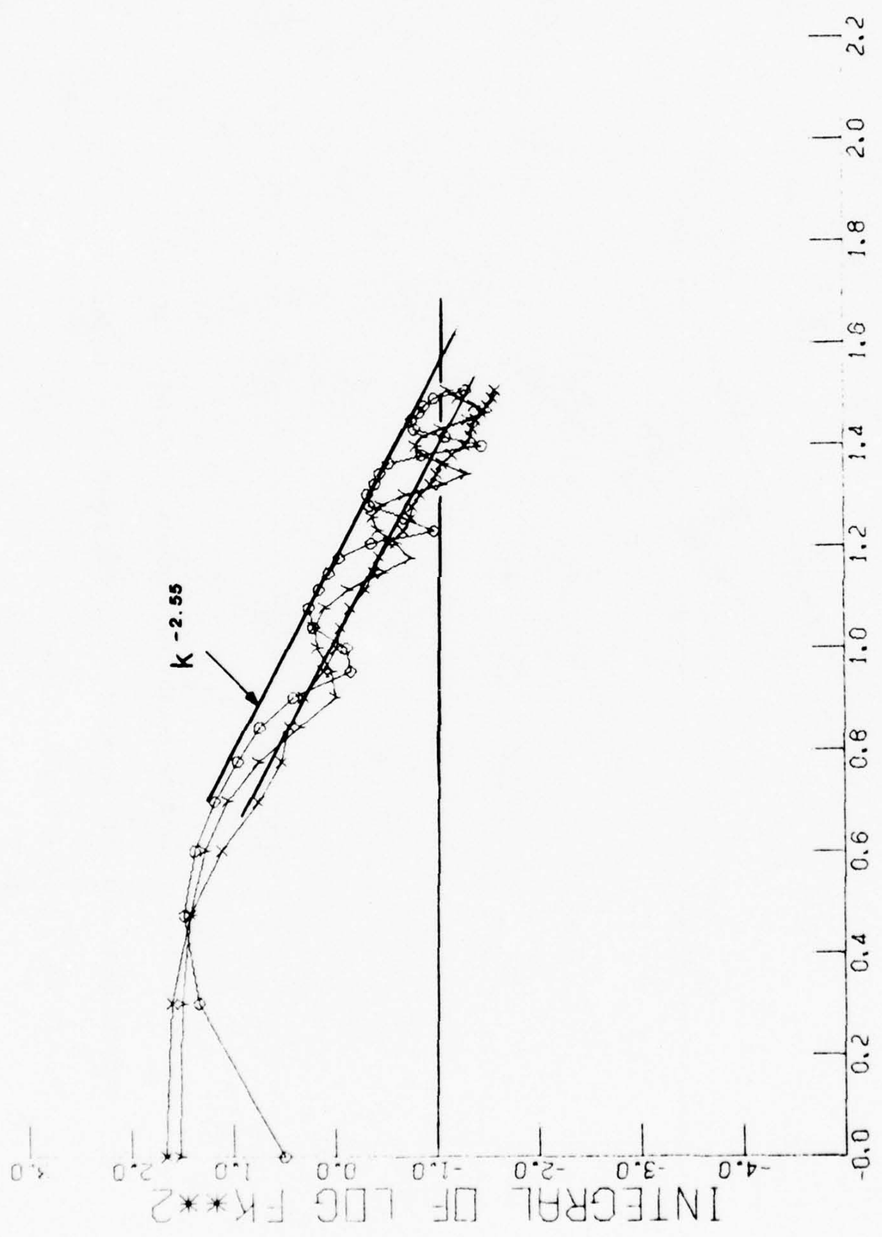

Fig. 17 — Discrete one-dimensional energy spectra (X, Y and O) for a *rectangular* figure *rotated* at 30° to the x-axis. $2a_x = 2b_x = 15$, $2a_y = 2b_y = 7$ and $(2N)^2 = 64^2$.

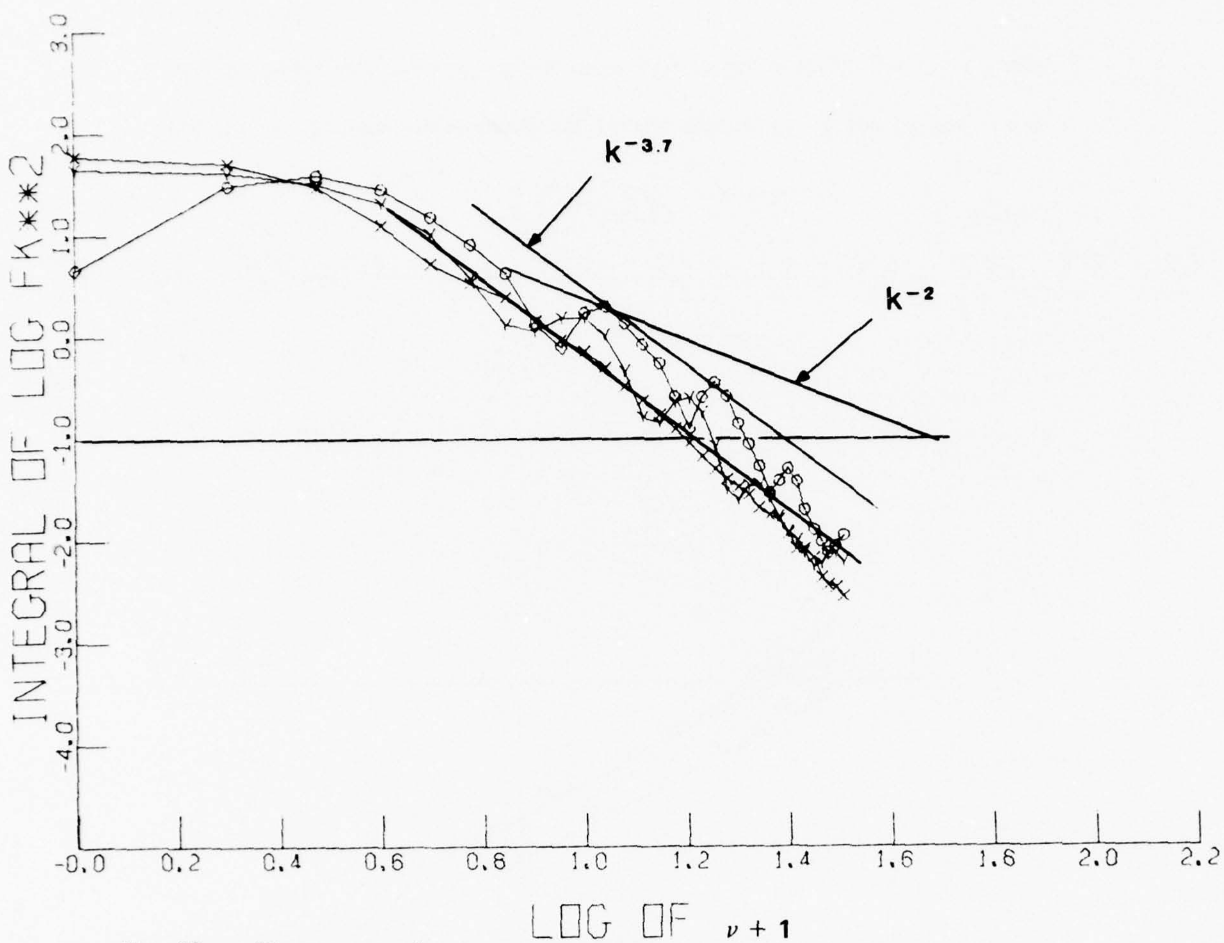

Fig. 18 — Discrete one-dimensional energy spectra (X, Y and O) for a trapezoidal figure (Fig. 7c) *rotated* at 30° to the x-axis. $A = 1$, $2a_x = 15$, $2b_x = 19$, $2a_y = 7$, $2b_y = 11$ and $(2N)^2 = 64^2$.

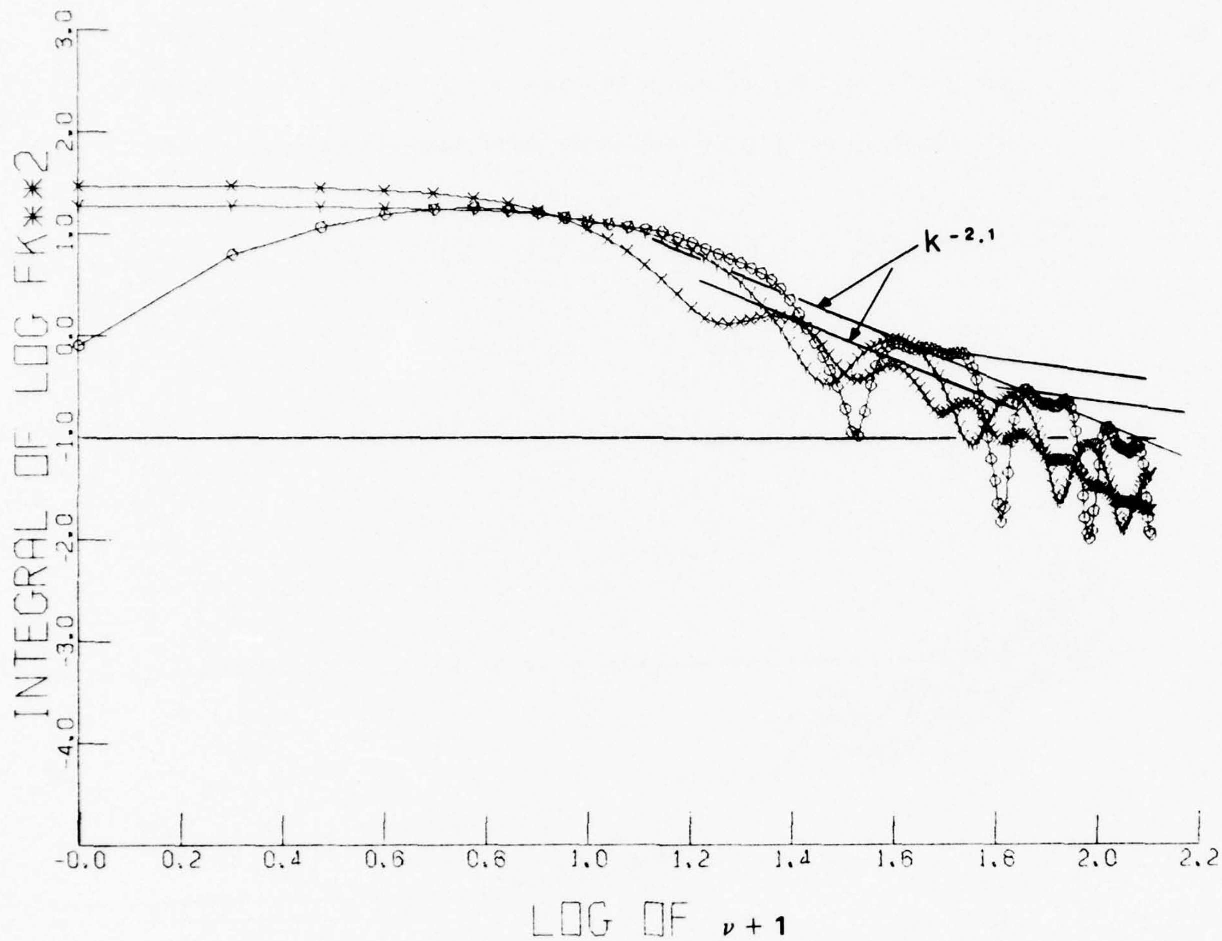

Fig. 19 — Discrete one-dimensional energy spectra (X, Y and O) for two *rectangular* figures at 30° to the x-axis as shown in Fig. 7d. $L_s = O$ and $(2N)^2 = 256^2$.

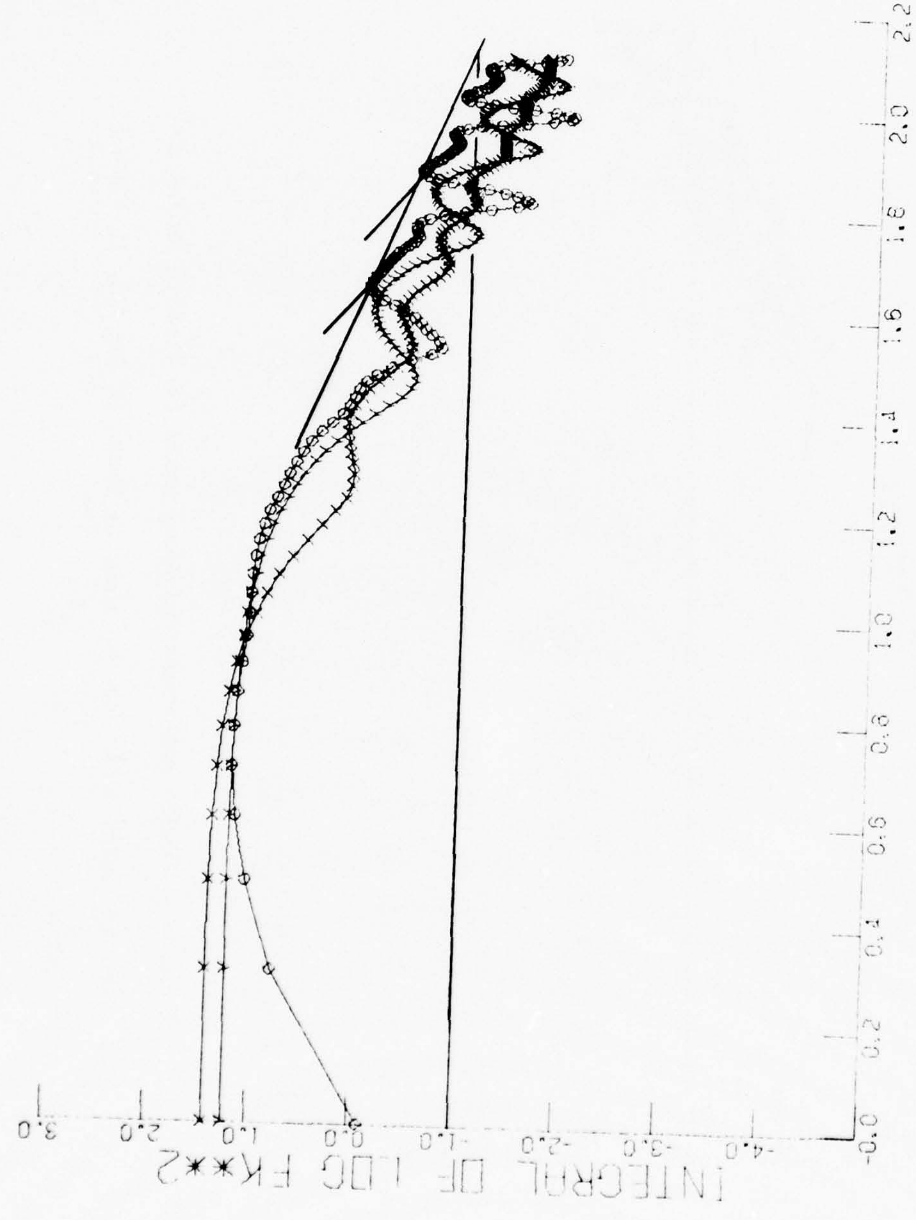

Fig. 20 — Discrete one-dimensional energy spectra (X, Y and O) for two *rectangular* figures at 30° to the x-axis as shown in Fig. 7d. $L_s = 2$ and $(2N)^2 = 256^2$.

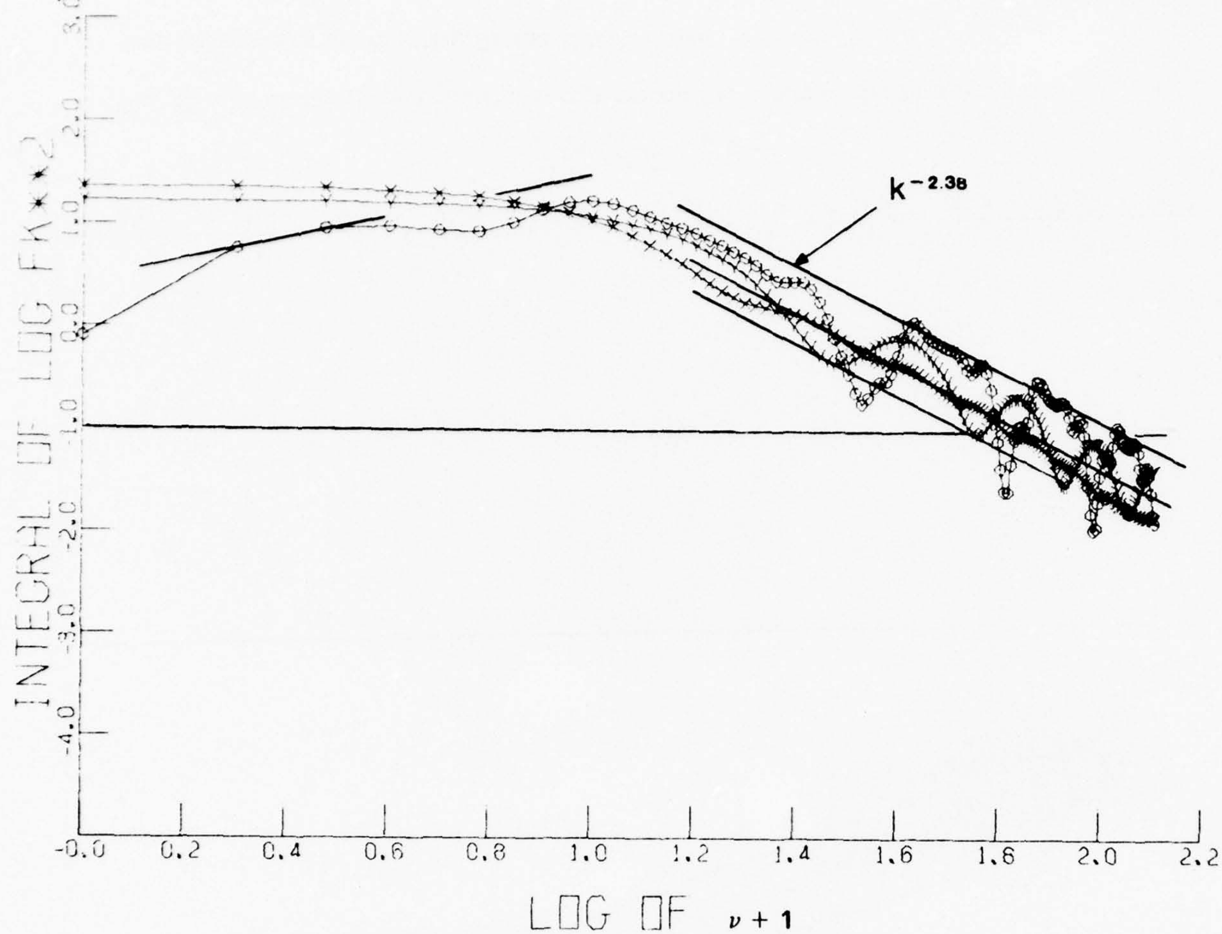

Fig. 21 — Discrete one-dimensional energy spectra (X, Y and O) for two *rectangular* figures at 30° to the x-axis as shown in Fig. 7d. $L_s = 16$ and $(2N)^2 = 256^2$.

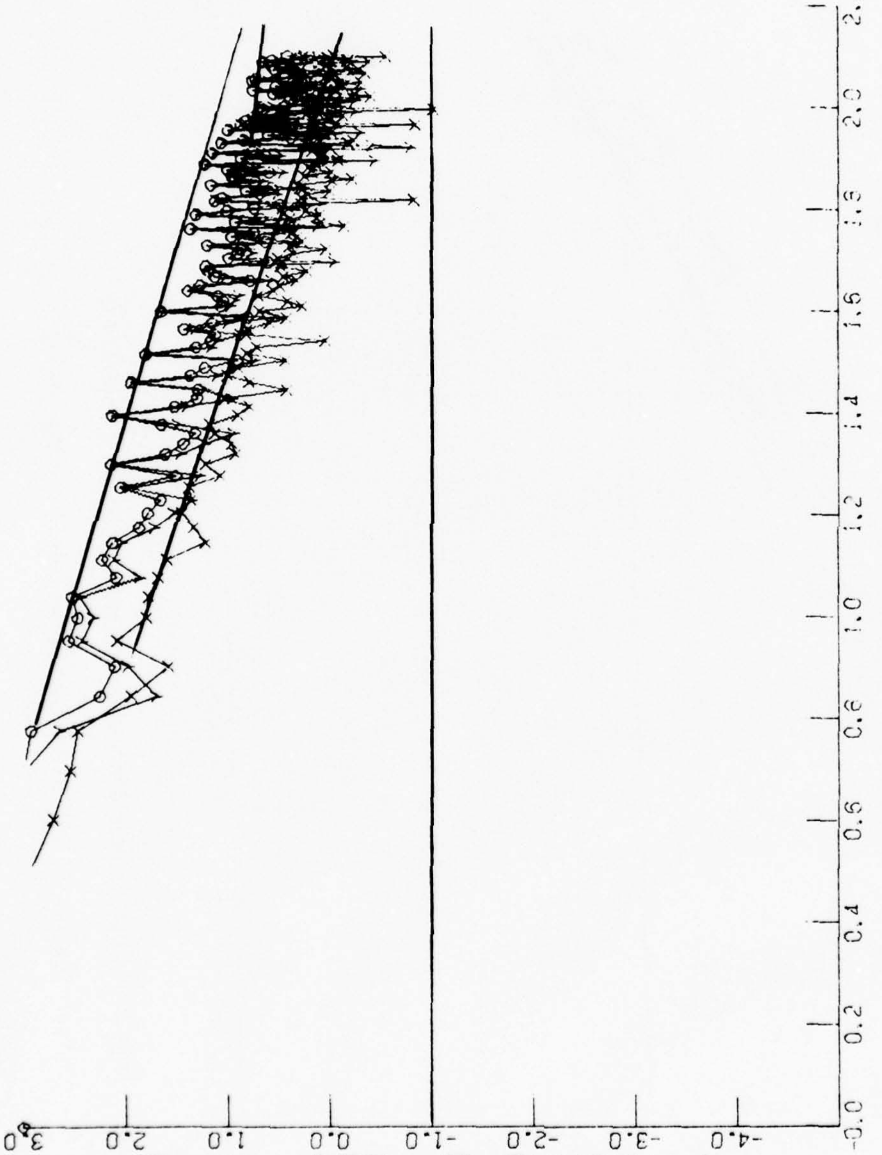

Fig. 22 — Discrete one-dimensional energy spectra (*X*, *Y* and *O*) for four *rectangular* figures as shown in Fig. 7e and $(2N)^2 = 256^2$.

DISTRIBUTION LIST

DEPARTMENT OF DEFENSE

ASSISTANT SECRETARY OF DEFENSE
COMM, CMD, CONT & INTELL
WASHINGTON, D.C. 20301
    01CY ATTN J. BABCOCK
    01CY ATTN M. EPSTEIN

ASSISTANT TO THE SECRETARY OF DEFENSE
ATOMIC ENERGY
WASHINGTON, D.C. 20301
    01CY ATTN EXECUTIVE ASSISTANT

DIRECTOR
COMMAND CONTROL TECHNICAL CENTER
PENTAGON RM BE 685
WASHINGTON, D.C. 20301
    01CY ATTN C-650
    01CY ATTN C-312 R. MASON

DIRECTOR
DEFENSE ADVANCED RSCH PROJ AGENCY
ARCHITECT BUILDING
1400 WILSON BLVD.
ARLINGTON, VA. 22209
    01CY ATTN NUCLEAR MONITORING RESEARCH
    01CY ATTN STRATEGIC TECH OFFICE

DEFENSE COMMUNICATION ENGINEER CENTER
1860 WIEHLE AVENUE
RESTON, VA. 22090
    01CY ATTN CODE R820
    01CY ATTN CODE R410 JAMES W. MCLEAN
    01CY ATTN CODE R720 J. WORTHINGTON

DIRECTOR
DEFENSE COMMUNICATIONS AGENCY
WASHINGTON, D.C. 20305
        (ADR CNWDI: ATTN CODE 240 FOR)
    01CY ATTN CODE 480
    01CY ATTN CODE 810 R. W. ROSTRON
    01CY ATTN CODE 101B
    01CY ATTN CODE 103 M. RAFFENSPERGER

DEFENSE DOCUMENTATION CENTER
CAMERON STATION
ALEXANDRIA, VA. 22314
    (12 COPIES IF OPEN PUBLICATION, OTHERWISE 2 COPIES)
    12CY ATTN TC

DIRECTOR
DEFENSE INTELLIGENCE AGENCY
WASHINGTON, D.C. 20301
    01CY ATTN DT-1B
    01CY ATTN DB-4C E. O'FARRELL
    01CY ATTN DIAAP A. WISE
    01CY ATTN DIAST-5
    01CY ATTN DT-1BZ R. MORTON
    01CY ATTN HQ-TR J. STEWART
    01CY ATTN W. WITTIG DC-7D

DIRECTOR
DEFENSE NUCLEAR AGENCY
WASHINGTON, D.C. 20305
    01CY ATTN STVL
    04CY ATTN TITL
    01CY ATTN DDST
    03CY ATTN RAAE

COMMANDER
FIELD COMMAND
DEFENSE NUCLEAR AGENCY
KIRTLAND AFB, NM 87115
    01CY ATTN FCPR

DIRECTOR
INTERSERVICE NUCLEAR WEAPONS SCHOOL
KIRTLAND AFB, NM 87115
    01CY ATTN DOCUMENT CONTROL

JOINT CHIEFS OF STAFF
WASHINGTON, D.C. 20301
    01CY ATTN J-3 WWMCCS EVALUATION OFFICE

DIRECTOR
JOINT STRAT TGT PLANNING STAFF
OFFUTT AFB
OMAHA, NB 68113
    01CY ATTN JLTW-2
    01CY ATTN JPST G. GOETZ

CHIEF
LIVERMORE DIVISION FLD COMMAND DNA
DEPARTMENT OF DEFENSE
LAWRENCE LIVERMORE LABORATORY
P. O. BOX 808
LIVERMORE, CA 94550
    01CY ATTN FCPRL

DIRECTOR
NATIONAL SECURITY AGENCY
DEPARTMENT OF DEFENSE
FT. GEORGE G. MEADE, MD 20755
    01CY ATTN JOHN SKILLMAN R52
    01CY ATTN FRANK LEONARD
    01CY ATTN W14 PAT CLARK
    01CY ATTN OLIVER H. BARTLETT W32
    01CY ATTN R5

COMMANDANT
NATO SCHOOL (SHAPE)
APO NEW YORK 09172
    01CY ATTN U.S. DOCUMENTS OFFICER

UNDER SECY OF DEF FOR RSCH & ENGRG
DEPARTMENT OF DEFENSE
WASHINGTON, D.C. 20301
    01CY ATTN STRATEGIC & SPACE SYSTEMS (OS)

WWMCCS SYSTEM ENGINEERING ORG
WASHINGTON, D.C. 20305
    01CY ATTN R. CRAWFORD

COMMANDER/DIRECTOR
ATMOSPHERIC SCIENCES LABORATORY
U.S. ARMY ELECTRONICS COMMAND
WHITE SANDS MISSILE RANGE, NM 88002
    01CY ATTN DELAS-EO F. NILES

DIRECTOR
BMD ADVANCED TECH CTR
HUNTSVILLE OFFICE
P. O. BOX 1500
HUNTSVILLE, AL 35807
    01CY ATTN ATC-T MELVIN T. CAPPS
    01CY ATTN ATC-O W. DAVIES
    01CY ATTN ATC-R DON RUSS

PROGRAM MANAGER
BMD PROGRAM OFFICE
5001 EISENHOWER AVENUE
ALEXANDRIA, VA 22333
    01CY ATTN DACS-BMT J. SHEA

CHIEF C-E SERVICES DIVISION
U.S. ARMY COMMUNICATIONS CMD
PENTAGON RM 1B269
WASHINGTON, D.C. 20310
    01CY ATTN C-E-SERVICES DIVISION

COMMANDER
FRADCOM TECHNICAL SUPPORT ACTIVITY
DEPARTMENT OF THE ARMY
FORT MONMOUTH, N.J. 07703
01CY ATTN DRSEL-NL-RD H. BENNET
01CY ATTN DRSEL-PL-ENV H. BOMKE
01CY ATTN J. E. QUIGLEY

COMMANDER
HARRY DIAMOND LABORATORIES
DEPARTMENT OF THE ARMY
2800 POWDER MILL ROAD
ADELPHI, MD 20783
(CNWDI-INNER ENVELOPE: ATTN: DELHD-RBH)
01CY ATTN DELHD-TI M. WEINER
01CY ATTN DELHD-RB R. WILLIAMS
01CY ATTN DELHD-NP F. WIMENITZ
01CY ATTN DELHD-NP C. MOAZED

COMMANDER
U.S. ARMY COMM-ELEC ENGRG INSTAL AGY
FT. HUACHUCA, AZ 85613

01CY ATTN CCC-EMEO GEORGE LANE

COMMANDER
U.S. ARMY FOREIGN SCIENCE & TECH CTR
220 7TH STREET, NE
CHARLOTTESVILLE, VA 22901
01CY ATTN DRXST-SD
01CY ATTN R. JONES

COMMANDER
U.S. ARMY MATERIEL DEV & READINESS CMD
5001 EISENHOWER AVENUE
ALEXANDRIA, VA 22333
01CY ATTN DRCLDC J. A. BENDER

COMMANDER
U.S. ARMY NUCLEAR AND CHEMICAL AGENCY
7500 BACKLICK ROAD
BLDG 2073
SPRINGFIELD, VA 22150
01CY ATTN LIBRARY

DIRECTOR
U.S. ARMY BALLISTIC RESEARCH LABS
ABERDEEN PROVING GROUND, MD 21005
01CY ATTN TECH LIB EDWARD BAICY

COMMANDER
U.S. ARMY SATCOM AGENCY
FT. MONMOUTH, NJ 07703
01CY ATTN DOCUMENT CONTROL

COMMANDER
U.S. ARMY MISSILE INTELLIGENCE AGENCY
REDSTONE ARSENAL, AL 35809
01CY ATTN JIM GAMBLE

DIRECTOR
U.S. ARMY TRADOC SYSTEMS ANALYSIS ACTIVITY
WHITE SANDS MISSILE RANGE, NM 88002
01CY ATTN ATAA-SA
01CY ATTN TCC/F. PAYAN JR.
01CY ATTN ATAA-TAC LTC J. HESSE

COMMANDER
NAVAL ELECTRONIC SYSTEMS COMMAND
WASHINGTON, D.C. 20360
01CY ATTN NAVALEX 034 T. HUGHES
01CY ATTN PME 117
01CY ATTN PME 117-T
01CY ATTN CODE 5011

COMMANDING OFFICER
NAVAL INTELLIGENCE SUPPORT CTR
4301 SUITLAND ROAD, BLDG. 5
WASHINGTON, D.C. 20390
01CY ATTN MR. DUBBIN STIC 12
01CY ATTN NISC-50
01CY ATTN CODE 5404 J. GALET

COMMANDER
NAVAL OCEAN SYSTEMS CENTER
SAN DIEGO, CA 92152
03CY ATTN CODE 532 W. MOLER
01CY ATTN CODE 0230 C. BAGGETT
01CY ATTN CODE 81 R. EASTMAN

DIRECTOR
NAVAL RESEARCH LABORATORY
WASHINGTON, D.C. 20375
01CY ATTN CODE 6700 TIMOTHY P. COFFEY (25 CYS IF UNCLASS, 1 CY IF CLASS)
01CY ATTN CODE 6701 JACK D. BROWN
01CY ATTN CODE 6780 BRANCH HEAD (150 CYS IF UNCLASS, 1 CY IF CLASS)
01CY ATTN CODE 7500 HQ COMM DIR BRUCE WALD
01CY ATTN CODE 7550 J. DAVIS
01CY ATTN CODE 7580
01CY ATTN CODE 7551
01CY ATTN CODE 7555
01CY ATTN CODE 6730 E. MCLEAN
01CY ATTN CODE 7127 C. JOHNSON

COMMANDER
NAVAL SEA SYSTEMS COMMAND
WASHINGTON, D.C. 20362
01CY ATTN CAPT R. PITKIN

COMMANDER
NAVAL SPACE SURVEILLANCE SYSTEM
DAHLGREN, VA 22448
01CY ATTN CAPT J. H. BURTON

OFFICER-IN-CHARGE
NAVAL SURFACE WEAPONS CENTER
WHITE OAK, SILVER SPRING, MD 20910
01CY ATTN CODE F31

DIRECTOR
STRATEGIC SYSTEMS PROJECT OFFICE
DEPARTMENT OF THE NAVY
WASHINGTON, D.C. 20376
01CY ATTN NSP-2141
01CY ATTN NSSP-2722 FRED WIMBERLY

NAVAL SPACE SYSTEM ACTIVITY
P. O. BOX 92960
WORLDWAY POSTAL CENTER
LOS ANGELES, CALIF. 90009
01CY ATTN A. B. HAZZARD

COMMANDER
NAVAL SURFACE WEAPONS CENTER
DAHLGREN LABORATORY
DAHLGREN, VA 22448
    01CY ATTN CODE DF-14 R. BUTLER

COMMANDING OFFICER
NAVY SPACE SYSTEMS ACTIVITY
P.O. BOX 92960
WORLDWAY POSTAL CENTER
LOS ANGELES, CA. 90009
    01CY ATTN CODE 52

OFFICE OF NAVAL RESEARCH
ARLINGTON, VA 22217
    01CY ATTN CODE 465
    01CY ATTN CODE 461
    01CY ATTN CODE 402
    01CY ATTN CODE 420
    01CY ATTN CODE 421

COMMANDER
AEROSPACE DEFENSE COMMAND/DC
DEPARTMENT OF THE AIR FORCE
ENT AFB, CO 80912
    01CY ATTN DC MR. LONG

COMMANDER
AEROSPACE DEFENSE COMMAND/XPD
DEPARTMENT OF THE AIR FORCE
ENT AFB, CO 80912
    01CY ATTN XPDQQ
    01CY ATTN XP

AIR FORCE GEOPHYSICS LABORATORY
HANSCOM AFB, MA 01731
    01CY ATTN OPR HAROLD GARDNER
    01CY ATTN OPR-1 JAMES C. ULWICK
    01CY ATTN LKB KENNETH S. W. CHAMPION
    01CY ATTN OPR ALVA T. STAIR
    01CY ATTN PHP JULES AARONS
    01CY ATTN PHD JURGEN BUCHAU
    01CY ATTN PHD JOHN P. MULLEN

AF WEAPONS LABORATORY
KIRTLAND AFB, NM 87117
    01CY ATTN SUL
    01CY ATTN CA ARTHUR H. GUENTHER
    01CY ATTN DYC CAPT J. BARRY
    01CY ATTN DYC JOHN M. KAMM
    01CY ATTN DYT CAPT MARK A. FRY
    01CY ATTN DES MAJ GARY GANONG
    01CY ATTN DYC J. JANNI

AFTAC
PATRICK AFB, FL 32925
    01CY ATTN TF/MAJ WILEY
    01CY ATTN TN

AIR FORCE AVIONICS LABORATORY
WRIGHT-PATTERSON AFB, OH 45433
    01CY ATTN AAD WADE HUNT
    01CY ATTN AAD ALLEN JOHNSON

DEPUTY CHIEF OF STAFF
RESEARCH, DEVELOPMENT, & ACQ
DEPARTMENT OF THE AIR FORCE
WASHINGTON, D.C. 20330
    01CY ATTN AFRDQ

HEADQUARTERS
ELECTRONIC SYSTEMS DIVISION/XR
DEPARTMENT OF THE AIR FORCE
HANSCOM AFB, MA 01731
    01CY ATTN XR J. DEAS

HEADQUARTERS
ELECTRONIC SYSTEMS DIVISION/YSEA
DEPARTMENT OF THE AIR FORCE
HANSCOM AFB, MA 01731
    01CY ATTN YSEA

HEADQUARTERS
ELECTRONIC SYSTEMS DIVISION/DC
DEPARTMENT OF THE AIR FORCE
HANSCOM AFB, MA 01731
    01CY ATTN DCKC MAJ J. C. CLARK

HEADQUARTERS
ELECTRONIC SYSTEMS DIVISION, AFSC
HANSCOM AFB, MA 01731
    01CY ATTN XRW
    01CY ATTN JAMES WHELAN

COMMANDER
FOREIGN TECHNOLOGY DIVISION, AFSC
WRIGHT-PATTERSON AFB, OH 45433
    01CY ATTN NICD LIBRARY
    01CY ATTN ETDP B. BALLARD

COMMANDER
ROME AIR DEVELOPMENT CENTER, AFSC
GRIFFISS AFB, NY 13441
    01CY ATTN DOC LIBRARY/TSLD
    01CY ATTN OCSE V. COYNE

SAMSO/SZ
POST OFFICE BOX 92960
WORLDWAY POSTAL CENTER
LOS ANGELES, CA 90009
(SPACE DEFENSE SYSTEMS)
    01CY ATTN SZJ

STRATEGIC AIR COMMAND/XPFS
OFFUTT AFB, NB 68113
01CY ATTN XPFS MAJ B. STEPHAN
01CY ATTN ADWATE MAJ BRUCE BAUER
01CY ATTN NRT
01CY ATTN DOK CHIEF SCIENTIST

SAMSO/YA
P. O. BOX 92960
WORLDWAY POSTAL CENTER
LOS ANGELES, CA 90009
01CY ATTN YAT CAPT L. BLACKWELDER

SAMSO/SK
P. O. BOX 92960
WORLDWAY POSTAL CENTER
LOS ANGELES, CA 90009
01CY ATTN SKA (SPACE COMM SYSTEMS) M. CLAVIN

SAMSO/MN
NORTON AFB, CA 92409
(MINUTEMAN)
01CY ATTN MNNL LTC KENNEDY

COMMANDER
ROME AIR DEVELOPMENT CENTER, AFSC
HANSCOM AFB, MA 01731
01CY ATTN EEP A. LORENTZEN

DEPARTMENT OF ENERGY

DEPARTMENT OF ENERGY
ALBUQUERQUE OPERATIONS OFFICE
P. O. BOX 5400
ALBUQUERQUE, NM 87115
01CY ATTN DOC CON FOR D. SHERWOOD

DEPARTMENT OF ENERGY
LIBRARY ROOM G-042
WASHINGTON, D.C. 20545
01CY ATTN DOC CON FOR A. LABOWITZ

EG&G, INC.
LOS ALAMOS DIVISION
P. O. BOX 809
LOS ALAMOS, NM 85544
01CY ATTN DOC CON FOR J. BREEDLOVE

UNIVERSITY OF CALIFORNIA
LAWRENCE LIVERMORE LABORATORY
P. O. BOX 808
LIVERMORE, CA 94550
01CY ATTN DOC CON FOR TECH INFO DEPT
01CY ATTN DOC CON FOR L-389 R. OTT
01CY ATTN DOC CON FOR L-31 R. HAGER
01CY ATTN DOC CON FOR L-46 F. SEWARD

LOS ALAMOS SCIENTIFIC LABORATORY
P. O. BOX 1663
LOS ALAMOS, NM 87545
01CY ATTN DOC CON FOR J. WOLCOTT
01CY ATTN DOC CON FOR R. F. TASCHEK
01CY ATTN DOC CON FOR E. JONES
01CY ATTN DOC CON FOR J. MALIK
01CY ATTN DOC CON FOR R. JEFFRIES
01CY ATTN DOC CON FOR J. ZINN
01CY ATTN DOC CON FOR P. KEATON
01CY ATTN DOC CON FOR D. WESTERVELT

SANDIA LABORATORIES
P. O. BOX 5800
ALBUQUERQUE, NM 87115
01CY ATTN DOC CON FOR J. MARTIN
01CY ATTN DOC CON FOR W. BROWN
01CY ATTN DOC CON FOR A. THORNBROUGH
01CY ATTN DOC CON FOR T. WRIGHT
01CY ATTN DOC CON FOR D. DAHLGREN
01CY ATTN DOC CON FOR 3141
01CY ATTN DOC CON FOR SPACE PROJECT DIV

SANDIA LABORATORIES
LIVERMORE LABORATORY
P. O. BOX 969
LIVERMORE, CA 94550
    01CY ATTN DOC CON FOR B. MURPHEY
    01CY ATTN DOC CON FOR T. COOK

OFFICE OF MILITARY APPLICATION
DEPARTMENT OF ENERGY
WASHINGTON, D.C. 20545
    01CY ATTN DOC CON FOR D. GALE

OTHER GOVERNMENT

CENTRAL INTELLIGENCE AGENCY
ATTN RD/SI, RM 5G48, HQ BLDG
WASHINGTON, D.C. 20505
    01CY ATTN OSI/PSID RM 5F 19

DEPARTMENT OF COMMERCE
NATIONAL BUREAU OF STANDARDS
WASHINGTON, D.C. 20234
    (ALL CORRES: ATTN SEC OFFICER FOR)
    01CY ATTN R. MOORE

DEPARTMENT OF TRANSPORTATION
OFFICE OF THE SECRETARY
TAD-44.1, ROOM 10402-B
400 7TH STREET, S.W.
WASHINGTON, D.C. 20590
    01CY ATTN R. LEWIS
    01CY ATTN R. DOHERTY

INSTITUTE FOR TELECOM SCIENCES
NATIONAL TELECOMMUNICATIONS & INFO ADMIN
BOULDER, CO 80303
    01CY ATTN A. JEAN (UNCLASS ONLY)
    01CY ATTN W. UTLAUT
    01CY ATTN D. CROMBIE
    01CY ATTN L. BERRY

NATIONAL OCEANIC & ATMOSPHERIC ADMIN
ENVIRONMENTAL RESEARCH LABORATORIES
DEPARTMENT OF COMMERCE
BOULDER, CO 80302
    01CY ATTN R. GRUBB
    01CY ATTN AERONOMY LAB G. REID

NASA
GODDARD SPACE FLIGHT CENTER
GREENBELT, MD 20771
    01CY ATTN P. CORRIGAN

DEPARTMENT OF DEFENSE CONTRACTORS

AEROSPACE CORPORATION
P. O. BOX 92957
LOS ANGELES, CA 90009
    01CY ATTN I. GARFUNKEL
    01CY ATTN T. SALMI
    01CY ATTN V. JOSEPHSON
    01CY ATTN S. BOWER
    01CY ATTN N. STOCKWELL
    01CY ATTN D. OLSEN
    01CY ATTN J. CARTER
    01CY ATTN F. MORSE
    01CY ATTN SMFA FOR PWW

ANALYTICAL SYSTEMS ENGINEERING CORP
5 OLD CONCORD ROAD
BURLINGTON, MA 01803
    01CY ATTN RADIO SCIENCES

BERKELEY RESEARCH ASSOCIATES, INC.
P. O. BOX 983
BERKELEY, CA 94701
    01CY ATTN J. WORKMAN

BOEING COMPANY, THE
P. O. BOX 3707
SEATTLE, WA 98124
    01CY ATTN G. KEISTER
    01CY ATTN D. MURRAY
    01CY ATTN G. HALL
    01CY ATTN J. KENNEY

CALIFORNIA AT SAN DIEGO, UNIV OF
IPAPS, B-019
LA JOLLA, CA 92093
    01CY ATTN HENRY G. BOOKER

BROWN ENGINEERING COMPANY, INC.
CUMMINGS RESEARCH PARK
HUNTSVILLE, AL 35807
    01CY ATTN ROMEO A. DELIBERIS

CHARLES STARK DRAPER LABORATORY, INC.
555 TECHNOLOGY SQUARE
CAMBRIDGE, MA 02139
    01CY ATTN D. B. COX
    01CY ATTN J. P. GILMORE

COMPUTER SCIENCES CORPORATION
6565 ARLINGTON BLVD
FALLS CHURCH, VA 22046
    01CY ATTN H. BLANK
    01CY ATTN JOHN SPOOR
    01CY ATTN C. NAIL

COMSAT LABORATORIES
LINTHICUM ROAD
CLARKSBURG, MD 20734
01CY ATTN G. HYDE

CORNELL UNIVERSITY
DEPARTMENT OF ELECTRICAL ENGINEERING
ITHACA, NY 14850
01CY ATTN D. T. FARLEY JR

ELECTROSPACE SYSTEMS, INC.
BOX 1359
RICHARDSON, TX 75080
01CY ATTN H. LOGSTON
01CY ATTN SECURITY (PAUL PHILLIPS)

ESL INC.
495 JAVA DRIVE
SUNNYVALE, CA 94086
01CY ATTN J. ROBERTS
01CY ATTN JAMES MARSHALL
01CY ATTN C. W. PRETTIE

FORD AEROSPACE & COMMUNICATIONS CORP
3939 FABIAN WAY
PALO ALTO, CA 94303
01CY ATTN J. T. MATTINGLEY

GENERAL ELECTRIC COMPANY
SPACE DIVISION
VALLEY FORGE SPACE CENTER
GODDARD BLVD KING OF PRUSSIA
P. O. BOX 8555
PHILADELPHIA, PA 19101
01CY ATTN M. H. BORTNER SPACE SCI LAB

GENERAL ELECTRIC COMPANY
P. O. BOX 1122
SYRACUSE, NY 13201
01CY ATTN F. REIBERT

GENERAL ELECTRIC COMPANY
TEMPO-CENTER FOR ADVANCED STUDIES
816 STATE STREET (P.O. DRAWER QQ)
SANTA BARBARA, CA 93102
01CY ATTN DASIAC
01CY ATTN DON CHANDLER
01CY ATTN TOM BARRETT
01CY ATTN TIM STEPHANS
01CY ATTN WARREN S. KNAPP
01CY ATTN WILLIAM MCNAMARA
01CY ATTN B. GAMBILL
01CY ATTN MACK STANTON

GENERAL ELECTRIC TECH SERVICES CO., INC.
HMES
COURT STREET
SYRACUSE, NY 13201
01CY ATTN G. MILLMAN

GENERAL RESEARCH CORPORATION
SANTA BARBARA DIVISION
P. O. BOX 6770
SANTA BARBARA, CA 93111
    01CY ATTN JOHN ISE JR
    01CY ATTN JOEL GARBARINO

GEOPHYSICAL INSTITUTE
UNIVERSITY OF ALASKA
FAIRBANKS, AK 99701
    (ALL CLASS ATTN: SECURITY OFFICER)
    01CY ATTN T. N. DAVIS (UNCL ONLY)
    01CY ATTN NEAL BROWN (UNCL ONLY)
    01CY ATTN TECHNICAL LIBRARY

GTE SYLVANIA, INC.
ELECTRONICS SYSTEMS GRP-EASTERN DIV
77 A STREET
NEEDHAM, MA 02194
    01CY ATTN MARSHAL CROSS

ILLINOIS, UNIVERSITY OF
DEPARTMENT OF ELECTRICAL ENGINEERING
URBANA, IL 61803
    01CY ATTN K. YEH

ILLINOIS, UNIVERSITY OF
107 COBLE HALL
801 S. WRIGHT STREET
URBANA, IL 60680
    (ALL CORRES ATTN SECURITY SUPERVISOR FOR)
    01CY ATTN K. YEH

INSTITUTE FOR DEFENSE ANALYSES
400 ARMY-NAVY DRIVE
ARLINGTON, VA 22202
    01CY ATTN J. M. AEIN
    01CY ATTN ERNEST BAUER
    01CY ATTN HANS WOLFHARD
    01CY ATTN JOEL BENGSTON

HSS, INC.
2 ALFRED CIRCLE
BEDFORD, MA 01730
    01CY ATTN DONALD HANSEN

INTL TEL & TELEGRAPH CORPORATION
500 WASHINGTON AVENUE
NUTLEY, NJ 07110
    01CY ATTN TECHNICAL LIBRARY

JAYCOR
1401 CAMINO DEL MAR
DEL MAR, CA 92014
    01CY ATTN S. R. GOLDMAN

JOHNS HOPKINS UNIVERSITY
APPLIED PHYSICS LABORATORY
JOHNS HOPKINS ROAD
LAUREL, MD 20810
    01CY ATTN DOCUMENT LIBRARIAN
    01CY ATTN THOMAS POTEMRA
    01CY ATTN JOHN DASSOULAS

LOCKHEED MISSILES & SPACE CO INC
P. O. BOX 504
SUNNYVALE, CA 94088
    01CY ATTN DEPT 60-12
    01CY ATTN D. R. CHURCHILL

LOCKHEED MISSILES AND SPACE CO INC
3251 HANOVER STREET
PALO ALTO, CA 94304
    01CY ATTN MARTIN WALT DEPT 52-10
    01CY ATTN RICHARD G. JOHNSON DEPT 52-12
    01CY ATTN W. L. IMHOF DEPT 52-12

KAMAN SCIENCES CORP
P. O. BOX 7463
COLORADO SPRINGS, CO 80933
    01CY ATTN T. MEAGHER

LINKABIT CORP
10453 ROSELLE
SAN DIEGO, CA 92121
    01CY ATTN IRWIN JACOBS

LOWELL RSCH FOUNDATION, UNIVERSITY OF
450 AIKEN STREET
LOWELL, MA 01854
    01CY ATTN K. BIBL

M.I.T. LINCOLN LABORATORY
P. O. BOX 73
LEXINGTON, MA 02173
    01CY ATTN DAVID M. TOWLE
    01CY ATTN P. WALDRON
    01CY ATTN L. LOUGHLIN
    01CY ATTN D. CLARK

MARTIN MARIETTA CORP
ORLANDO DIVISION
P. O. BOX 5837
ORLANDO, FL 32805
    01CY ATTN R. HEFFNER

MCDONNELL DOUGLAS CORPORATION
5301 BOLSA AVENUE
HUNTINGTON BEACH, CA 92647
    01CY ATTN N. HARRIS
    01CY ATTN J. MOULE
    01CY ATTN GEORGE MROZ
    01CY ATTN W. OLSON
    01CY ATTN R. W. HALPRIN
    01CY ATTN TECHNICAL LIBRARY SERVICES

MISSION RESEARCH CORPORATION
735 STATE STREET
SANTA BARBARA, CA 93101
    01CY ATTN P. FISCHER
    01CY ATTN W. F. CREVIER
    01CY ATTN STEVEN L. GUTSCHE
    01CY ATTN D. SAPPENFIELD
    01CY ATTN R. BOGUSCH
    01CY ATTN R. HENDRICK
    01CY ATTN RALPH KILB
    01CY ATTN DAVE SOWLE
    01CY ATTN F. FAJEN
    01CY ATTN M. SCHEIBE
    01CY ATTN CONRAD L. LONGMIRE
    01CY ATTN WARREN A. SCHLUETER

MITRE CORPORATION, THE
P. O. BOX 208
BEDFORD, MA 01730
    01CY ATTN JOHN MORGANSTERN
    01CY ATTN G. HARDING
    01CY ATTN C. E. CALLAHAN

MITRE CORP
WESTGATE RESEARCH PARK
1820 DOLLY MADISON BLVD
MCLEAN, VA 22101
    01CY ATTN W. HALL
    01CY ATTN W. FOSTER

PACIFIC-SIERRA RESEARCH CORP
1456 CLOVERFIELD BLVD.
SANTA MONICA, CA 90404
    01CY ATTN E. C. FIELD JR

PENNSYLVANIA STATE UNIVERSITY
IONOSPHERE RESEARCH LAB
318 ELECTRICAL ENGINEERING EAST
UNIVERSITY PARK, PA 16802
    (NO CLASSIFIED TO THIS ADDRESS)
    01CY ATTN IONOSPHERIC RESEARCH LAB

PHOTOMETRICS, INC.
442 MARRETT ROAD
LEXINGTON, MA 02173
    01CY ATTN IRVING L. KOFSKY

PHYSICAL DYNAMICS INC.
P. O. BOX 3027
BELLEVUE, WA 98009
    01CY ATTN E. J. FREMOUW

PHYSICAL DYNAMICS INC.
P. O. BOX 1069
BERKELEY, CA 94701
    01CY ATTN A. THOMPSON

R & D ASSOCIATES
P. O. BOX 9695
MARINA DEL REY, CA 90291
    01CY ATTN FORREST GILMORE
    01CY ATTN BRYAN GABBARD
    01CY ATTN WILLIAM B. WRIGHT JR
    01CY ATTN ROBERT F. LELEVIER
    01CY ATTN WILLIAM J. KARZAS
    01CY ATTN H. ORY
    01CY ATTN C. MACDONALD
    01CY ATTN R. TURCO

RAND CORPORATION, THE
1700 MAIN STREET
SANTA MONICA, CA 90406
    01CY ATTN CULLEN CRAIN
    01CY ATTN ED BEDROZIAN

RIVERSIDE RESEARCH INSTITUTE
80 WEST END AVENUE
NEW YORK, NY 10023
    01CY ATTN VINCE TRAPANI

SCIENCE APPLICATIONS, INC.
P. O. BOX 2351
LA JOLLA, CA 92038
    01CY ATTN LEWIS M. LINSON
    01CY ATTN DANIEL A. HAMLIN
    01CY ATTN D. SACHS
    01CY ATTN E. A. STRAKER
    01CY ATTN CURTIS A. SMITH
    01CY ATTN JACK MCDOUGALL

RAYTHEON CO.
528 BOSTON POST ROAD
SUDBURY, MA 01776
    01CY ATTN BARBARA ADAMS

SCIENCE APPLICATIONS, INC.
HUNTSVILLE DIVISION
2109 W. CLINTON AVENUE
SUITE 700
HUNTSVILLE, AL 35805
    01CY ATTN DALE H. DIVIS

SCIENCE APPLICATIONS, INCORPORATED
8400 WESTPARK DRIVE
MCLEAN, VA 22101
    01CY ATTN J. COCKAYNE

SCIENCE APPLICATIONS, INC.
80 MISSION DRIVE
PLEASANTON, CA 94566
    01CY ATTN SZ

SRI INTERNATIONAL
333 RAVENSWOOD AVENUE
MENLO PARK, CA 94025
    01CY ATTN DONALD NEILSON
    01CY ATTN ALAN BURNS
    01CY ATTN G. SMITH
    01CY ATTN L. L. COBB
    01CY ATTN DAVID A. JOHNSON
    01CY ATTN WALTER G. CHESNUT
    01CY ATTN CHARLES L. RINO
    01CY ATTN WALTER JAYE
    01CY ATTN M. BARON
    01CY ATTN RAY L. LEADABRAND
    01CY ATTN G. CARPENTER
    01CY ATTN G. PRICE
    01CY ATTN J. PETERSON
    01CY ATTN R. HAKE, JR.
    01CY ATTN V. GONZALES
    01CY ATTN D. MCDANIEL

TECHNOLOGY INTERNATIONAL CORP
75 WIGGINS AVENUE
BEDFORD, MA 01730
    01CY ATTN W. P. BOQUIST

TRW DEFENSE & SPACE SYS GROUP
ONE SPACE PARK
REDONDO BEACH, CA 90278
    01CY ATTN R. K. PLEBUCH
    01CY ATTN S. ALTSCHULER
    01CY ATTN D. DEE

VISIDYNE, INC.
19 THIRD AVENUE
NORTH WEST INDUSTRIAL PARK
BURLINGTON, MA 01803
    01CY ATTN CHARLES HUMPHREY
    01CY ATTN J. W. CARPENTER